

**CHAIN EXCHANGE KINETICS OF BLOCK COPOLYMER MICELLES
MEDIATED BY THE AIR-WATER INTERFACE**

by

Laurens Heusele

A thesis submitted to the Faculty of the University of Delaware in partial fulfillment of the requirements for the degree of Master of Chemical Engineering

Spring 2017

© 2017 Laurens Heusele
All Rights Reserved

**CHAIN EXCHANGE KINETICS OF BLOCK COPOLYMER MICELLES
MEDIATED BY THE AIR-WATER INTERFACE**

by

Laurens Heusele

Approved: _____
Thomas H. Epps, III, Ph.D.
Professor in charge of thesis on behalf of the Advisory Committee

Approved: _____
Millicent O. Sullivan, Ph.D.
Professor in charge of thesis on behalf of the Advisory Committee

Approved: _____
Abraham M. Lenhoff, Ph.D.
Chair of the Department of Chemical and Biomolecular Engineering

Approved: _____
Babatunde A. Ogunnaike, Ph.D.
Dean of the College of Engineering

Approved: _____

Ann L. Ardis, Ph.D.

Senior Vice Provost for Graduate and Professional Education

ACKNOWLEDGMENTS

First and foremost, I would like to thank my advisors for guiding me through this project and offering their expertise. Through all the difficulties and setbacks that come along with research, their help and insights are what made this thesis possible. I want to thank Emma for embarking on this journey with me. From applying for a visa to discussing experimental results, our conversations and mutual support strongly helped me along the way. I wish to thank the Epps and Sullivan group members for offering helping hands during my time here, in particular Priyanka and Melody for sticking through our Dutch conversations and making this experience more enjoyable. I would like to thank Shu and Chad for training and assisting us in the lab. I want to thank Kathie Young for helping me out more times than I could keep track of and Norm Wagner, Isabelle Benoit and Peter Van Puyvelde for advising us through the application procedures. Special thanks go out to the many friends I made here at the University of Delaware, for making me feel at home and making this the adventure of a lifetime.

Most importantly, I want to thank my family and friends for being there for me. In particular, my parents and sisters for believing in me and for tolerating my lack of communication during my time abroad. It is a comforting feeling to know there are people that will always support you through your journey in life.

TABLE OF CONTENTS

LIST OF TABLES	vii
LIST OF FIGURES	viii
ABSTRACT	xi

Chapter

1	INTRODUCTION	1
1.1	Formation of Micelles	3
1.2	Micellar Structure	4
1.3	Thermodynamics of Micellization	7
1.4	Kinetics of Micelles.....	10
1.4.1	Single Chain Exchange.....	12
1.4.2	Fusion/Fission.....	13
1.4.3	Shear Induced Flocculation and Interfacial Nucleation	14
1.4.4	Influencing chain exchange	16
1.5	Applications of block copolymer micelles	17
1.5.1	Drug delivery vehicles.....	17
1.5.2	Metal Encapsulating Nanoparticles	18
1.5.3	Surface modifiers.....	19
1.6	Thesis Overview	19
	REFERENCES	21
2	MATERIALS AND METHODS	25
2.1	Materials	25
2.2	Solution methods	31
2.3	Preparation of micelle solutions	32
2.4	Temperature control	36
2.5	Interface control.....	36
2.6	Characterization.....	38
2.6.1	Dynamic Light Scattering.....	40

2.6.2	Fitting the correlation function	42
2.6.3	Equipment and procedures	44
	REFERENCES	45
3	RESULTS AND DISCUSSION.....	47
3.1	Cosolvent method.....	48
3.2	Bimodal size distribution.....	51
3.3	Interface mediated micelle growth	54
3.3.1	Varying bulk to interface turnover rate	54
3.3.2	Varying concentration	59
	REFERENCES	61
4	THESIS OVERVIEW AND FUTURE RECOMMENDATIONS	62
4.1	Conclusion.....	62
4.2	Future recommendations	63
	REFERENCES	66
Appendix		
	COPYRIGHT PERMISSION STATEMENT	67

LIST OF TABLES

Table 2.1:	Properties of the 1,4-polybutadiene- <i>b</i> -poly(ethylene oxide) reported by Polymer Source. The molar ratios were obtained by analyzing the nuclear magnetic resonance (NMR) spectrum, with M_n the number average molecular weight and M_w the weight average molecular weight.	27
Table 2.2:	Molar ratios of the PB-PEO sample determined with ^1H NMR.....	28
Table 2.3:	Molar ratios of the PB-PEO sample determined with ^1H NMR.....	30
Table 2.4:	Properties of the polymer determined by ^1H NMR and GPC before and after fractionation. The information provided by Polymer Source is listed for comparison.	31
Table 2.5:	Concentrations of the polymer solutions before and after dialysis.	35
Table 3.1:	The hydrodynamic radius Dh and polydispersity σ for direct dissolution and the cosolvent method. The hydrodynamic radius of the micelles decreased upon addition and removal of cosolvent.	49
Table 3.2:	The surface turnover rates and their respective ratio to the bulk for vials filled for 25%, 50% and 75%.....	57

LIST OF FIGURES

Figure 1.1: Differences between low molecular weight surfactant micelles (a) and block copolymer micelles (b). The solvophobic blocks, indicated in yellow, form the core of the micelle whereas the solvophilic blocks, in purple, form the corona.	2
Figure 1.2: Different morphologies obtained for varying values of the packing factor p . Depicted here are the structures obtained for packing factors ranging from 0 to 1. Note however, that packing factors can also be larger than 1, resulting in inverted micelles	5
Figure 1.3: Star-like (a) and crew-cut (b) type micelles.	6
Figure 1.4: Single chain exchange and fusion/fission as kinetic pathways for chain exchange in micelles.....	11
Figure 1.5: Shear induced flocculation and Interfacial nucleation as kinetic pathways for chain exchange in micelles.	11
Figure 2.1: Phase diagram for dilute solutions of poly(butadiene- <i>b</i> -ethylene oxide) block polymer amphiphiles. The polymer forms various morphologies including bilayer vesicles (B), cylindrical micelles (C), spherical micelles (S), and networks (N), depending on the molecular curvature of the amphiphile. The molecular curvature is controlled by the degree of polymerization of the hydrophobic block (N_{PB}) and hydrophilic weight fraction (w_{PEO}), and the desired solution morphology can be targeted by tuning the block polymer molecular weight and composition. The figure was reproduced from Jain and Bates, <i>Science</i> , 2003, 300, 460-464. The figure was reprinted with permission from AAAS. ³	26
Figure 2.2: GPC spectrum of the PB-PEO sample. The retention time can be related to the molecular weight by using the linear curve.	27
Figure 2.3: ¹ H NMR spectrum obtained from the polymer sample. The different peaks are indicated with letters that correspond to molecular structures represented in the top left corner.	28

Figure 2.4:	GPC spectrum of the PB-PEO sample after fractionation. The retention time can be related to the molecular weight by using the linear curve.	29
Figure 2.5:	¹ H NMR spectrum obtained from the polymer sample after fractionation. The different peaks are indicated with letters that correspond to molecular structures represented in the top left corner.	30
Figure 2.6:	Solution preparation of the micelle solutions using the cosolvent method. After 3 days of stirring in water, THF is added. After a subsequent 3 days of stirring, dialysis is performed to remove the THF from the cores of the micelles.	33
Figure 2.7:	Dialysis of polymer solution with deionized water. While the polymer is not allowed to travel through the membrane, THF and water can freely interchange.	34
Figure 2.8:	Calibration curve for PB-PEO solutions in water at $\lambda = 259\text{nm}$	35
Figure 2.9:	Graphical representation of the rotator device spinning counterclockwise. The green arrows indicate creation of interface whereas the red arrows represent a collapse.	37
Figure 2.10:	A Venn-diagram showing the advantages and disadvantages of the different characterization methods. DLS is relatively low cost and offers good statistical certainty but lacks proper structure resolution. Cryo-TEM is mid-cost and provides good structure resolution whereas DLS cannot. The drawback, however, is the poor statistical certainty when used for quantitative analysis. Lastly, SANS gives both good structure resolution and statistical certainty but comes at a high cost.	39
Figure 2.11:	DLS on micelle solutions with as output a more fluctuation intensity for smaller particles (a) with respect to larger particles (b).	41
Figure 3.1:	Autocorrelation functions for the cosolvent method (red) and direct dissolution (blue) using the quadratic cumulant fit in MATLAB. Note that the autocorrelation data was normalized for ease of comparison. The larger size of the micelles present in the direct dissolution sample corresponds to a delayed exponential decay.	49
Figure 3.2:	Size evolution of a 2.5 mg mL^{-1} PB-PEO sample after dialysis. The solution was vortex mixed for 30 minutes. The error bars were obtained by taking triplicate DLS measurements of the sample.	50

- Figure 3.3: The autocorrelation data of a 2.5 mg mL^{-1} PB-PEO sample being vortex mixed for 15 minutes with the quadratic cumulant (a) and the polydisperse double exponential (b). The RMSE for both methods over a time period of 30 minutes is given in (c). The error bars were obtained by taking triplicate DLS measurements of the sample. 52
- Figure 3.4: The change of the intensity weight coefficient C_2 over time for a 2.5 mg mL^{-1} sample being vortex mixed for 30 minutes (a). The corresponding polydispersities of the two populations σ_1 and σ_2 along with the polydispersity obtained from the QC are given in (b). The error bars were obtained by taking triplicate DLS measurements of the sample. 53
- Figure 3.5: Micelle size evolution for samples with 25% filled vials (yellow diamonds), 50% filled vials (blue triangles) and 75% filled vials (green squares), with C_2 the intensity weight coefficient obtained from the PDE fit. The samples were vortex mixed for 30 min total. The error bars were obtained by taking triplicate DLS measurements of the sample. Note that the error bars are sometimes smaller than the marker size and therefore not always visible. 55
- Figure 3.6: Dimensions of the vial. Note that the thickness of the vial (= 1mm) has to be taken into account upon calculating the surface turnover rate. 56
- Figure 3.7: Micelle size evolution for samples with 25% filled vials (yellow diamonds), 50% filled vials (blue triangles) and 75% filled vials (green squares), with C_2 the intensity weight coefficient obtained from the PDE fit. The samples were rotated at 40 rpm. The error bars were obtained by taking triplicate DLS measurements of the sample. Note that the error bars are sometimes smaller than the marker size and therefore not always visible. 58
- Figure 3.8: Micelle size evolution for samples with 0.5 mg mL^{-1} (yellow diamonds) and 1.25 mg mL^{-1} (blue triangles), with C_2 the intensity weight coefficient obtained from the PDE fit. The error bars were obtained by taking triplicate DLS measurements of the sample. Note that the error bars are sometimes smaller than the marker size and therefore not always visible. 60

ABSTRACT

The self-assembly of amphiphilic block copolymer micelles has been the center of extensive research due to their broad set of applications. Many of the applications, such as drug delivery vehicles, hinge on the stability of the micelles and how they interact with their environment. In expanding the knowledge of these nanostructures and their behavior, novel technologies can be further explored. However, despite their use in a wide range of fields, the fundamental growth mechanisms at work remain mostly unresolved. The work in this thesis focuses on the influence of the air-water interface on micellar growth. The system consists of poly(1,4-butadiene-*b*-ethylene oxide) in aqueous solvent. In order to examine the relaxation behavior, the system is perturbed from its equilibrium state by addition and removal of cosolvent (tetrahydrofuran). Dynamic light scattering is chosen as a primary characterization tool to monitor the micelle sizes over time as it offers a cheap and fast way to investigate trends before moving on to costlier techniques. A distinct difference in chain exchange was found for vortex mixed samples with varying interface turnover rate to bulk volume ratios, suggesting an interface mediated growth mechanism. Additionally, the same experiment was repeated on a rotator to obtain a more quantifiable result, however, yielding a less pronounced difference. Lastly, the concentration dependency of the micelle growth kinetics was investigated. The examined concentrations exhibited an equal growth, in agreement with the hypothesis of interfacial nucleation. Overall, the data gathered from the rotator experiments appeared noisy, making it hard to justify any conclusions. Nonetheless, the results

presented in this thesis agree with the proposed role of the interface in the kinetic pathway. Understanding this process unlocks interesting new possibilities in utilizing block copolymers such as cargo exchange between drug delivery vehicles.

Chapter 1

INTRODUCTION

For the last 40 years, amphiphilic block copolymers have been of wide interest due to their unique properties. Their ability to self-assemble into a diverse set of nanostructures makes them desirable in a number of industries such as biomedical applications,¹ pharmaceuticals,² catalysts and electronics³ among many others. Amphiphilic block copolymers are macromolecules in which a hydrophilic polymer block is covalently linked to a hydrophobic polymer block. Their spontaneous formation of ordered structures is similar to that of low molecular weight surfactants but offers some key advantages due to their macromolecular nature. Advances in polymer chemistry have allowed for the controlled synthesis of numerous architectures of block copolymers such as linear, star-like and dendrites to name a few, each of which can lead to different micellar structures.⁴⁻⁸

In contrast to surfactant micelles, block copolymer micelles are known to have slow exchange kinetics. The highly unfavorable interactions between the solvophobic block and the solvent lead to a high activation energy, which scales with the size of the solvophobic block.^{9,10} Investigating the growth kinetics for these types of micelles can be challenging considering the wide range of lifetime. Another consequence of these slow exchange kinetics is pathway dependency, meaning that processing conditions have an impact on the resulting nanostructures and properties.

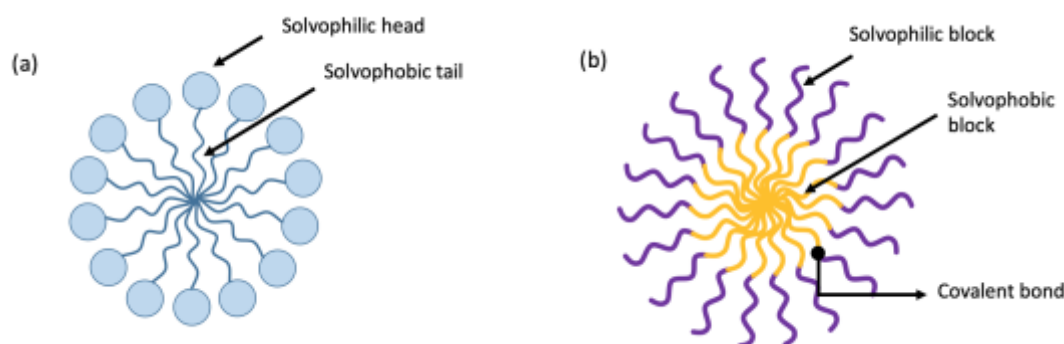


Figure 1.1: Differences between low molecular weight surfactant micelles (a) and block copolymer micelles (b). The solvophobic blocks, indicated in yellow, form the core of the micelle whereas the solvophilic blocks, in purple, form the corona.

Common characterization methods for nanoparticles are cryogenic transmission electron microscopy (cryo-TEM) and small angle neutron scattering (SANS). While both of these techniques offer a very useful data output, they can be expensive and time intensive. Dynamic light scattering (DLS) offers a fast way to investigate trends before moving on to costlier techniques.

Understanding the behavior of micelles and their growth is crucial for their applications. Even though block copolymer micelles have been studied for an extensive period of time, the chain exchange kinetics are still not fully understood. Recent work showed the importance of the air-water interface as a mediator for micelle to exchange chains,¹¹ opening up new possibilities for cargo exchange between drug delivery vehicles.

This chapter aims to provide background knowledge on block copolymer micelles and their potential as well as to clarify the purpose and motivation for this thesis. More specifically, the different subjects touched upon are the formation of

micelles (1.1), micellar structures (1.2), thermodynamics of micellization (1.3), kinetics of micellization (1.4), applications for block copolymer micelles (1.5) and a thesis overview (1.6).

1.1 Formation of Micelles

Self-assembly is the process in which molecules order themselves into microstructures. When immersed in a selective solvent, *i.e.*, a solvent that selectively dissolves one of the blocks, amphiphilic molecules are known to spontaneously form a wide range of nanostructures. In aqueous solutions, the hydrophilic part of a block copolymer will form a surrounding shell or corona, shielding the hydrophobic core from the solvent to minimize unfavorable interactions.⁷ This process closely relates to the micelle formation of low molecular weight surfactants. Macromolecular micelles tend to be more stable and exhibit a lower critical micelle concentration (CMC) with respect to surfactants. Furthermore, their slow dissociation rate allows for the retention of the loaded drugs.¹² This property is important for applications such as drug delivery, in which the micellar system is diluted upon entering biological fluids and premature release of the drugs is prohibited by the stability of the micelles. In order to fully exploit the properties of the nanostructures, control of this self-assembly process is required, which can be done internally or externally. The former implies adapting the particle interactions which can provide, for example, directionality. External ways to tailor the self-assembly process include electric or magnetic fields and deformation.¹⁴

The concentration at which self-assembly initiates is called the CMC. Upon reaching the CMC, addition of block copolymers will increase the number of micelles whereas the concentration of unimers in solution remains constant.⁵ Measuring the

surface tension offers a practical approach of determining this critical concentration. For polymeric micelles, the CMC is also referred to as critical aggregation concentration (CAC).

1.2 Micellar Structure

In order to investigate the properties of micelles, it is important to understand their structure. Amphiphilic molecules are known to self-assemble into spheres, cylinders, vesicles, and bilayers, see Figure 1.2. The resulting morphology is dependent on the relative sizes of the hydrophobic and hydrophilic blocks.^{7,8,15} The packing parameter, p , characterizes the block-size ratio and can be used to determine the resulting structure from the block copolymer blocks. This parameter consists out of the interfacial area between the two blocks, a_0 , the length of the insoluble block *i.e.*, the hydrophobic block in an aqueous solvent, l_c , and the volume of the insoluble block, v . For different ranges of p , different structures are obtained.^{7,8}

$$p = \frac{v}{a_0 l_c} \quad (1.1)$$

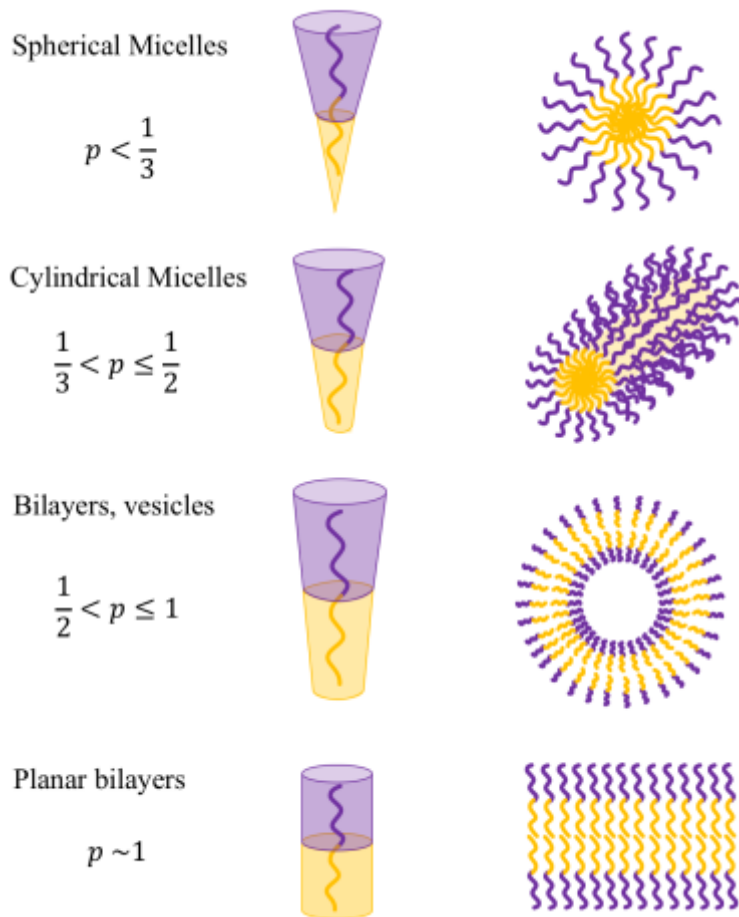


Figure 1.2: Different morphologies obtained for varying values of the packing factor p . Depicted here are the structures obtained for packing factors ranging from 0 to 1. Note however, that packing factors can also be larger than 1, resulting in inverted micelles

For the purpose of this thesis, spherical micelles are desired. Therefore, this structure will be discussed more in depth. A spherical micelle can be divided into two main parts, the core and the corona. The core consists out of the insoluble blocks of the copolymer, surrounded by the corona or shell. Two boundary cases of the micelle structures can be described: star-like or hairy, and crew-cut.^{5,7} The star-like

configuration embodies a small core surrounded by a large corona *i.e.*, the radius of the core, R_c , is much smaller than the thickness of the corona, L . Conversely, the crew-cut structure has a core radius much larger than the corona thickness. These structures are depicted in Figure 1.3.

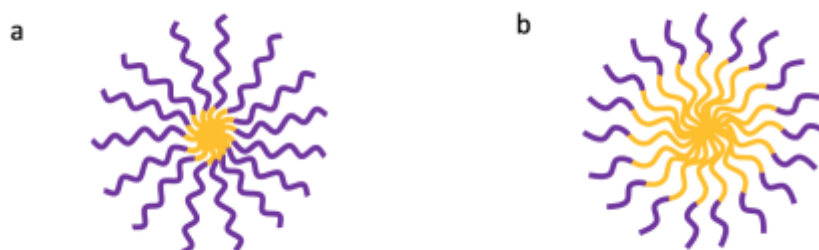


Figure 1.3: Star-like (a) and crew-cut (b) type micelles.

Other properties such as the aggregation number P , which describes the number of unimers in the micelle, the grafting distance, the hydrodynamic radius, R_h , and the radius of gyration, R_g , are impacted by the block sizes as well as the Flory-Huggins interaction parameter, χ .⁷

In addition to micelles composed from a single block copolymer, it is possible to form blended micelles from multiple copolymers. This technique has previously been used to discover new morphologies.^{16,17} New developments investigate the possibility to use blended micelles as substitutes for pure micelles. In contrast to needing a custom synthesis for a specific copolymer, blending a known set of copolymers can yield micelles with the same characteristics as the pure micelles. The blended micelles were reported to exhibit identical structural properties to the pure micelles with the same average composition.¹⁶

1.3 Thermodynamics of Micellization

Micellization and its thermodynamic equilibrium size are a result of balancing various forces. Hydrophilic, hydrophobic and, depending on the presence of charges, electrostatic interactions all influence the morphology.⁹ Understanding the thermodynamics of the micellization process allows for the estimation of various characteristics of micellar systems.

Micellization in organic solvent is a balance between enthalpic and entropic forces. The formation of nanostructures leads to a decrease in entropy, thereby increasing the free energy. On the other hand, polymer-solvent interactions are replaced by polymer-polymer and solvent-solvent interactions, leading to a decrease in enthalpy, *i.e.*, a negative ΔH value, and an overall decrease in Gibbs free energy.¹⁸

In aqueous medium micellization is no longer an enthalpic but an entropically driven process. The reason for this discrepancy is the hydrophobic effect, which characterizes the interactions of solvent molecules in the vicinity of the polymer.^{12,13} Water molecules are highly ordered around hydrophobic blocks of the copolymer in solution. Upon transition from unimers into micelles these molecules are set free, resulting in an entropic gain. The entropic decrease due the formation of an aggregate structure from unimers is negligible. This effect further implicates that an increasing length of the hydrocarbons results in a lower CAC.^{12,13}

When a micelle grows in size, it decreases the interfacial area to bulk ratio and therefore lowers the free energy. Conversely, when more unimers are present in the micelle, the steric hindrance in the corona increases. A larger aggregation number also translates to more stretching of the core and corona blocks, leading to a loss of conformational entropy.^{12,13} The equilibrium size of the micelles will result from a

trade-off between these forces. A well-known approximation of the equilibrium aggregation number is:¹⁹

$$P_{eq} \cong \left(\frac{2K_1}{3K_2} \frac{\gamma}{k_B T} \right)^{\frac{6}{5}} (N_A m)^{\frac{4}{5}} \quad (1.2)$$

with P_{eq} the equilibrium aggregation number, K_1 and K_2 coefficients, m the average volume per monomer, γ the interfacial tension, N_A the degree of polymerization of the hydrophilic block, k_B the Boltzmann constant and the temperature T .

Various theories have been proposed to describe the complex relations involved in this self-assembly process. The free energy can be analyzed by scaling and mean-field theories as well as computational simulations.

Pioneered by de Gennes, scaling theories provide a simple way of computing the free energy of micelle systems. Using power laws, relations between block copolymer and micellar properties are established. The models examined for this theory use the pseudo-phase approximation and a mixing energy that is assumed negligible.⁹ The free energy, per one block copolymer, of a micelle can be described as a sum of three parts: interfacial, core and corona free energy.

$$F_{micelle} = F_{interface} + F_{core} + F_{corona} \quad (1.3)$$

Interfacial tension has a great impact on the thermodynamics of the system and can be correlated to the interfacial free energy. This term promotes micelle growth and would lead to macro phase segregation if not countered by other forces, such as repulsion in the corona.

$$F_{interface} \sim P^{-\frac{1}{3}} \gamma \quad (1.4)$$

The free energy of the core and corona differs depending on the type of micelle. For spherical micelles, the two boundary cases, star-like and crew cut and additionally an intermediate case can be considered. Whereas crew-cut micelles have a large core with respect to the corona, $F_{core} \sim P^{2/3}$ will be the dominant term.⁹ The following relation is found using theories of de Gennes, with N_B the degree of polymerization of the insoluble block:⁷

$$P \sim \gamma N_B \quad (1.5)$$

In contrast to crew-cut micelles, the free energy of star-like and intermediate cases are predominately dependent on the free energy of the corona, for which the following relations are obtained:⁹

$$\frac{F_{corona}}{k_B T} \sim \begin{cases} P^{\frac{1}{2}} \ln \left(N_A^{\frac{2}{3}} P^{-\frac{2}{15}} N_B^{-\frac{1}{3}} \right) & (a) \\ P^{\frac{5}{18}} N_B^{-\frac{5}{9}} N_A & (b) \end{cases} \quad (1.6)$$

with (a) for star-like and (b) for intermediate. The scaling laws are based on the star polymer theory of Daoud and Cotton and were later found to be in agreement with findings of Halperin.^{7,9,10,20}

$$P \sim \begin{cases} \gamma^{\frac{6}{5}} N_B^{\frac{4}{5}} & (a) \\ \gamma^{\frac{18}{11}} N_B^2 N_A^{-\frac{18}{11}} & (b) \end{cases} \quad (1.7)$$

The simplicity of scaling theories make them an attractive way of processing thermodynamic properties of micellar systems. However, there are some drawbacks. The restrictions of scaling theories lie in the approximation of infinitely long polymers in a good solvent, and thus, not taking end-chain effects as well as interactions between the solvent and polymer into consideration. Mean-field theories can act as a complementary technique to account for these deficits.⁷

Leibler et al.²¹ and Noolandi et al.²² developed semianalytical mean-field theories of block copolymer micellization, finding good agreements between experimental and theoretical results. Further work by Nagarajan and Ganesh took the molar volumes of the solvent and the polymer blocks into account and demonstrated the influence of the A and B block on micellar properties:²³

$$P \sim N_A^{1.19} N_B^{-0.51} \quad (1.8)$$

Computational methods, mostly consisting of Monte Carlo-type simulations, have been reviewed by Binder and Muller²⁴ and Shelley and Shelly.²⁵ These methods are beneficial in that they use few approximations and are typically straightforward. A drawback is the computational load, resulting in simulation type methods that usually limit their block sizes.

1.4 Kinetics of Micelles

The complexities involved in micelle kinetics has prompted extensive research over the past decades. Initially, surfactant micelles were scrutinized by perturbing the system and characterizing the relaxation of the micelles. However, low molecular weight micelles behave very differently than micelles composed of macromolecules. The higher molecular weight results in slower kinetics which are characteristic for block copolymer micelles.^{4,5,7-9,12,16} The inherent glassiness of the micellar system makes the study of the chain exchange difficult as it leads to pathway dependency and requires sufficient agitation. A number of theories have been proposed to explain micellar growth, mainly by two main mechanisms: single chain exchange (1.4.1) and fusion/fission (1.4.2), (Figure 1.4):



Figure 1.4: Single chain exchange and fusion/fission as kinetic pathways for chain exchange in micelles.

Single chain exchange, initially proposed by Aniansson-Wall, describes a step-wise insertion and expulsion of molecules.⁴ The model was initially set up for low molecular weight surfactant molecules, after which Halperin and Alexander argued its validity for macromolecules.¹⁰ Kahlwei, Lessner and Teubner later incorporated growth by fusion/fission in their model.^{7,9} In addition to these two main processes, interfacial nucleation and shear induced flocculation (1.4.3) are also proposed as possible growth mechanisms, see Figure 1.5.

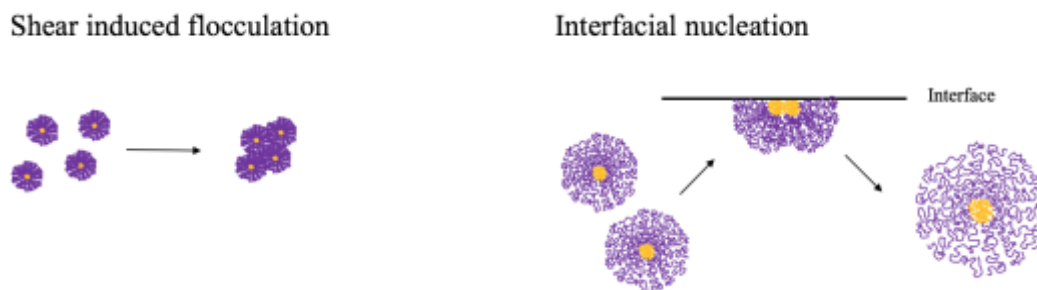


Figure 1.5: Shear induced flocculation and Interfacial nucleation as kinetic pathways for chain exchange in micelles.

1.4.1 Single Chain Exchange

One of the first and most notable theories on micelle chain exchange is that of Aniansson-Wall.²⁷ Due to steric hindrance considerations, their theory is limited to single chain exchange. Aniansson-Wall based their work on non-ionic low molecular weight micelles in a near equilibrium state. The insertion and expulsion of the unimers can be described as:^{4,9,26,27}



in which A_1 represents a unimer and A_p a micelle with aggregation number P . The rate constants for insertion and expulsion are k_i and k_e respectively. Additionally, a rate equation can be written as:

$$\frac{d[A_1]}{dt} = -k_i[A_p][A_1] + k_e[A_{p+1}] \quad (1.11)$$

Using these equations, the relaxation can be described by two relaxation constants τ_1 and τ_2 . The first constant is related to the fast relaxation, and decreases linearly with micelle concentration. The second relaxation time constant τ_2 is slower and has a more complex concentration dependency. The Aniansson-Wall model further suggests that the unimer chain exchange is limited by the expulsion rate constant.

Halperin and Alexander subsequently developed a theory that describes chain exchange kinetics for block copolymer micelles.¹⁰ Their findings argue that the predictions made by Aniansson-Wall can be extended to macromolecules. Correspondingly, chain exchange is proposed to be governed by single chain exchange and limited by the expulsion rate constant. The expulsion of a unimer is described as a two-stage process. First, the solvophobic block is emitted from the micelle core,

overcoming the main energetic barrier. Secondly, the entire unimer diffuses through the corona. The chain exchange can be written as a first-order kinetic process:^{4,9,10}

$$R(t) = \exp(k_e t) \sim \exp\left(-\frac{t}{\tau} \exp\left(-\frac{\gamma N_B}{k_B T}\right)\right) \quad (1.12)$$

with τ the characteristic time, γ the interfacial tension, k_B the Boltzmann constant and N_B the degree of polymerization of the hydrophobic block. The sensitivity of chain exchange to the size of the core block as a result of the unfavorable interactions is highlighted in this equation by the double exponential.

1.4.2 Fusion/Fission

A second mechanism for chain exchange is a fusion and fission based process. The micelles can collide to form a larger nanostructure (fusion) or divide up into smaller micelles (fission) which can be written as:



with A_i a micelle with aggregation number i . Both Aniansson-Wall as well as Halperin and Alexander argued that the energetic barrier was too high for this phenomenon to occur substantially.^{10,27} The activation energy was shown to heavily scale with the size of the hydrophobic block.⁹ These claims have been disputed by work of Dormidontova, who reasoned that the results obtained were only valid for small deviations from equilibrium.¹⁹ Additionally, the characteristic time for expulsion was overestimated and the disentanglement of the solvophobic block was not taken into consideration.¹⁹

Dormidontova further investigated the possibility of fusion and fission as a pathway for chain exchange by considering the free energy variation.¹⁹ A micelle with aggregation number P can split up into two micelles with aggregation number P_l and

P_2 (with $P_1 + P_2 = P$) and vice versa. The difference in free energy between an initial micelle and its constituent micelles as a result of fission can be written as:¹⁹

$$\Delta F = F_{P_1} + F_{P_2} - F_P \quad (1.14)$$

This equation expresses when fusion or fission is favorable, *i.e.*, a positive value for ΔF means fusion is favored while a negative value implies fission can lower the free energy. The equation can be reformed to:¹⁹

$$\Delta F = P^{\frac{3}{2}}(x^{\frac{3}{2}} + (1-x)^{\frac{3}{2}} - 1) + \frac{3}{2}P_{eq}^{\frac{5}{2}}P^{\frac{2}{3}}\left(x^{\frac{2}{3}} + (1-x)^{\frac{2}{3}} - 1\right) \quad (1.15)$$

with $x = \frac{P_1}{P}$ and P_{eq} the equilibrium aggregation number. From these

calculations, micelle fusion is proposed to be favorable for micelles of similar size with $P < \frac{3}{8}P_{eq}$ and for micelles of different size for which one of the micelles has an aggregation number $P > \frac{3}{8}P_{eq}$. Conversely, micelle fission is favored when a micelle has an aggregation number $P > \frac{3}{2}P_{eq}$. Important here is to note that Dormidontova's results imply that micelle fusion/fission is not negligible and can be a key pathway for micelle kinetics.^{9,19} Experiments performed on micelles perturbed far from equilibrium using cosolvent addition demonstrated a bimodal growth pattern, suggesting that fusion indeed occurs.²⁸

1.4.3 Shear Induced Flocculation and Interfacial Nucleation

Two alternative mechanisms for chain exchange are shear induced flocculation and interfacial nucleation. Flocculation is the process in which particles form clusters while maintaining their identity.¹³ This mechanism is a result of dispersion forces, causing particles to floc together (perikinetic flocculation).²⁹ Applying a shear flow can bring particles together more quickly than Brownian motion and is referred to as orthokinetic flocculation. The effect of shear induced flocculation has been scrutinized

using Couette flow experiments. The structure factor was scrutinized using Flow-SANS on a solution in rotating cylinders. No noticeable change was present, suggesting that shear induced flocculation is not occurring and that chain exchange is not solely related to shear.¹¹

The adsorption of nanoparticles at fluid-fluid interfaces, in this case air-water, has been used for a variety of applications. This phenomenon is induced by the decrease in free energy and is often irreversible. More quantitatively, the desorption energy of micelles is in the order of $1000 k_B T$.³⁰ Whereas these nanoparticles cannot desorb from the interface spontaneously, subjecting them to deformations at the interface by, for instance, mechanical rupturing can turn this process reversible. Additionally, it is important to have a high surface turnover rate as only a small percentage of micelles will be present at the interface with respect to the bulk.

The experimental finding that Couette flow does not induce chain exchange offered a first clue to the importance of the interface as a mediator for micelle kinetics.¹¹ If the interface were indeed the rate-limiting factor in this process, no dependency on concentration should be present, *i.e.*, a zero-order kinetics. Previous work has indicated this crucial role of the interface by vortex mixing micelle solutions of PB-PEO (polybutadiene-*b*-poly(ethylene oxide)) in water with varying concentrations.¹¹ Micelle fusion/fission as the controlling mechanism would lead to a second order kinetics. Using small angle neutron scattering (SANS), the extent of chain exchange was found to be the same and even decreasing for very high concentrations, strongly suggesting the validity of interfacial nucleation.¹¹

Generating a high surface turnover rate can be accomplished in multiple ways. Magnetic stirring as well as gas sparging the solution seemed to be insufficient in

unlocking this interfacial phenomenon in the micelle solutions.¹¹ Both are estimated to have a turnover rate of $\sim 1 \text{ cm}^2/\text{s}$. Conversely, vortex mixing is known to induce high shear stress and surface turnover rates. Simulations have estimated the turnover rate to be two orders of magnitude higher ($\sim 100 \text{ cm}^2/\text{s}$). Even though these approximations can differ from reality, they seem to be in relatively good agreement with experimental findings.¹¹ However, in order to properly quantify the amount of interface that is generated and destroyed, a more precise technique is required. A rotator can be used to precisely control and measure the interface present at each position. A surface turnover rate in the order of $\sim 10 \text{ cm}^2/\text{s}$ can be achieved, meaning the timescales for chain exchange will be somewhere in between that of magnetic stirring and vortex mixing. This device is further explained in section 2.3.

1.4.4 Influencing chain exchange

Probing chain exchange between block copolymer micelles requires awareness of the influencing parameters. Previous sections have partially discussed important factors, and a complete rendition of influencing chain exchange is given here.

First and foremost, agitation constitutes the most prominent method to unlock chain exchange in micelle solutions.^{9,11} Even when perturbed far from their equilibrium state, most block copolymer micelle systems will not exchange chains if not stirred, being effectively “frozen” in the selective solvent. Moving a system away from its equilibrium is a common practice to examine the relaxation behavior and can be accomplished by, for instance, cosolvent addition and removal or a temperature jump.

Equation 1.12 demonstrates the double exponential dependency on the interfacial tension, hydrophobic block size and temperature. As a result of this high

sensitivity, the chain exchange rate can be effectively increased by i) decreasing the size of the solvophobic block, ii) reducing the interfacial tension by tuning the compatibility of the core block and the solvent or iii) increasing the temperature.

Finally, it is important to note that the polymer of use should have a low dispersity, \bar{D} . Aside from yielding a narrow micelle size distribution, a low \bar{D} results in less deviation from the desired nanostructures. Additionally, the presence of homopolymer can retard chain exchange, highlighting the importance of purity of the material.³¹

1.5 Applications of block copolymer micelles

The unique features of block copolymers are used in an enormous number of applications. More specifically, block copolymer properties in micelles make them a very desirable material to work with. The low CMC that is inherent to block copolymer nanostructures is of vital importance in biological fluids, as would be the case for drug delivery vehicles (1.5.1).³² The high surface area of the nanostructures is used in applications such as metal encapsulating nanoparticles (1.5.2). Furthermore, block copolymer micelles can be used as tools for surface modification (1.5.3).

1.5.1 Drug delivery vehicles

Amphiphilic block copolymers and their self-assembling behavior offer a practical way of acting as a nanoscale shield for drugs. The wide variety of chemistries and morphologies involved with block copolymers makes it easy to tailor these ‘vehicles’ for specific purposes. For instance, the ability to adapt the sizes is important for cellular uptake efficiency, for which the maximum was obtained for nanocarriers of size 50 nm in several studies.³³ The exceptionally slow kinetics of micelles

composed from macromolecules make them even more suited for the job. Dilution in the blood can cause nanostructures to fall apart and prematurely release the drugs, which should be prohibited at all times. The goal is to trigger the micelle to disassemble at the right location. Some possible methods for controlled release involve a change of pH, applying light to photo-sensitive vehicles or changing the temperature. As stated by Kabanov et. al, three main systems can be considered concerning drug delivery.³⁴

The first drug loading systems are block copolymer micelles in which the drug is covalently attached to the copolymer. This technique is limited in that the copolymer blocks must be tailored specifically for each drug. The right functional groups and cleavable bonds have to be present to assure a successful release of the cargo.³⁵ Because of this drawback a second method, using solubilization, is a more preferred strategy. The drug is not covalently linked to the polymer, but is enclosed within the core of the micelle. It is important to note that the material being used for these types of drug delivery systems needs to be biocompatible or even biodegradable.² A third technique to mediate drug delivery is to use polyelectrolyte complexes composed out of cationic block copolymers and oligonucleotides. This relatively new technique is especially interesting for gene therapy applications.³⁶

1.5.2 Metal Encapsulating Nanoparticles

Aside from drugs, block copolymer micelles can also encapsulate metal salts as a cargo. One block requires selectivity for the metal while the other needs compatibility with the solvent. Once the metals are incorporated in the core of the micelle, they are chemically transformed into a disperse metal colloid. These nanoparticles bring with them very interesting catalytic or magnetic properties.³ This

type of drug delivery system is usually prepared in organic solvents but has been shown to work in aqueous media as well.³ The metal binding block is usually P4VP (poly(4-vinylpyridine)) or P2VP, covalently bonded to a solvent compatible block such as PEO (poly(ethylene oxide)) or PS (polystyrene).³

1.5.3 Surface modifiers

The ability of block copolymers to adsorb to surfaces has been exploited in many applications involving wetting, stabilization, improving biocompatibility etc. Micelles can also be useful for modifying surface properties, where they can either physically or chemically interact. A physical interaction consists of micelles adsorbing to the surface through the affinity of the solvent soluble block, thereby forming a micellar monolayer.³⁷ One potential application of these physical interactions is controlling the agglomeration process of latex.³⁸ Another use is stable micellar coating for non-fouling surfaces in the biomedical sector.¹

1.6 Thesis Overview

This thesis aims to investigate the role of the air-water interface in block copolymer micelle growth. Previous findings indicated the dependency of chain exchange kinetics on the interface turnover rate, prompting further quantification. In expanding the knowledge of these nanostructures and their behavior, novel technologies can be further explored.

A detailed description of the materials and methods can be found in Chapter 2. Furthermore, the processing conditions for solution preparation and characterization methods are reported and supported with a theoretical background. Chapter 3 discusses the results that were obtained using DLS measurements. The relationship

between micellar growth and the air-water interface was probed by characterizing samples with varying interface turnover rate to bulk volume ratios. Additionally, the dependency of chain exchange on concentration was explored. Finally, Chapter 4 summarizes the thesis work and future recommendations are made for the continuation of this project.

REFERENCES

1. Emoto, K.; Nagasaki, Y.; Iijima, M.; Kato, M.; Kataoka, K. Preparation of non-fouling surface through the coating with core-polymerized block copolymer micelles having aldehyde-ended PEG shell. *Colloids and Surfaces B: Biointerfaces*. **2000**, 18, 337–46.
2. Kwon, G.S.; Okano, T. Polymeric micelles as new drug carriers. *Advanced Drug Delivery Reviews* **1996**, 21, 107–16.
3. Bradley, J.S. The Chemistry of Transition Metal Colloids. In: *Cluster and colloids. From theory to application*. Schmid, G., Eds.; Wiley/VCH: Weinheim, 1994
4. Lund, R.; Willner, L.; Monkenbusch, M.; Panine, P.; Narayanan, T.; Colmenero, J.; Richter, D. Structural Observation and Kinetic Pathway in the Formation of Polymeric Micelles. *Physical Review Letters* **2009**, 102, 188301.
5. Gohy, J.F. Block Copolymer Micelles. *Advances in Polymer Science*. **2005**, 190, 65-136
6. Jensen, G. R.; Shi, Q.; Hernansanz, M.J.; Oliveira, C. L. P.; Deen, G. R.; Almdal, K.; Pedersen, J.S. Structure of PEP–PEO block copolymer micelles: exploiting the complementarity of small-angle X-ray scattering and static light scattering. *Journal of Applied Crystallography*. **2001**, 44, 473-482
7. Karayianni, M.; Pispas, S. Self-Assembly of Amphiphilic Block Copolymers in Selective Solvents. In *Fluorescence Studies of Polymer Containing Systems*. Karayianni, M.; Pispas, S.; Eds.; Procházka, K., 2016; pp 24-64
8. Smart, T.; Lomas, H.; M. Massignani, M.; Flores-merino, M.V.; Perez, L.R.; Battaglia, G. Block copolymer nanostructures One of the most important classes of synthetic systems for creating. **2008**, 3, 38–46

9. Lund, R.; Willner, L.; Richter, D. Kinetics of Block Copolymer Micelles Studied by Small-Angle Scattering Methods. *Advances in Polymer Science*. **2013**, 259, 51–158
10. Halperin, A. Polymeric Micelles: A Star Model. *Macromolecules*. **1987**, 20, 2943-2946
11. Murphy, R. P.; Kelley, E. G.; Rogers, S. A.; Sullivan, M.O.; Epps, T. H. Unlocking Chain Exchange in Highly Amphiphilic Block Polymer Micellar Systems: Influence of Agitation. *ACS Macro Letters*. **2014**, 3, 1106-1111
12. Kataoka, K.; Harada, A.; Nagasaki, Y. Block copolymer micelles for drug delivery: Design, characterization and biological significance. *Advanced Drug Delivery Reviews*. **2001**, 47, 113-131
13. Butt, H.J.; Graf, K.; Kappl, M. Physics and Chemistry of Interfaces. Eds.; Wiley/VCH: Weinheim, 1994
14. Grzelczak, M.; Vermant, J.; Furst, E. M.; Liz-Marzán, L. M. Directed self-assembly of nanoparticles. *ACS Nano*. **2010**, 4, 3591-3605
15. Goyal, P.S.; Aswal, V.K. Micellar structure and inter-micelle interactions in micellar solutions: Results of small angle neutron scattering studies. *Current Science*. **2001**, 80, 972-979
16. Wright, D. B.; Patterson, J. P.; Gianneschi, N. C.; Chassenieux, C.; O'Reilly, R. K. Polymer Chemistry obstacles of blending. *Polymer Chemistry*. **2016**, 7, 1577–1583
17. Wright, D. B.; Patterson, J. P.; Pitto-Barry, A.; Lu, A.; Kirby, N.; Gianneschi, N. C.; Chassenieux, C.; Colombani, O.; O'Reilly, R. K. The Copolymer Blending Method: A New Approach for Targeted Assembly of Micellar Nanoparticles. *Macromolecules*. **2015**, 48, 6516-6522
18. Price C. Colloidal properties of block copolymers. In *Developments in block copolymers*. Goodman, I., Eds.; Applied Science: London, 1982; pp. 39–79.
19. Dormidontova, E. E. Micellization kinetics in block copolymer solutions: scaling model *Macromolecules*, **1999**, 32, 7630–7644

20. Daoud, M.; Cotton J. P. Star-shaped polymers: a model for the conformation and its concentration dependence. *Journal de Physique*. **1982**, 43, 531–8.
21. Leibler, L.; Orland, H.; Wheeler, J. C. Theory of critical micelle concentration for solutions of block copolymers. *Journal Chemical Physics*. **1983**, 79, 3550–3557
22. Noolandi, J.; Hong, K. M. (1983) Theory of block copolymer micelles in solution. *Macromolecules*. **1983**, 16, 1443–1448
23. Nagarajan, R.; Ganesh, K. Block copolymer self-assembly in selective solvents: theory of solubilization in spherical micelles. *Macromolecules*, **1989**, 22, 4312–25
24. Binder, K.; Muller, M. Monte Carlo simulation of block copolymers. *Current Opinion in Colloid Interface Science*, **2000**, 5, 315–323
25. Shelley, J. C.; Shelley, M. Y. Computer simulation of surfactant solutions. *Current Opinion Colloid Interface Science*, **2000**, 5, 101–110
26. Lu, J. Mechanisms of Chain Exchange in Block Copolymer Micelles. Ph.D. Thesis, *University of Minnesota*, November 2015
27. Aniansson E. A. G.; Wall, S. N. On the Kinetics of Step-Wise Micelle Association. *The Journal of Physical Chemistry*. **1974**, 78, 1024–1030
28. Kelley, E. G.; Murphy, R. P.; Sepalla, J. E.; Smart, T. P.; Hann, S. D.; Sullivan, M. O.; Epps, T. H. Size evolution of highly amphiphilic macromolecular solution assemblies via a distinct bimodal pathway. *Nature Communications*. **2014**, 5, 3599
29. Mewis, J.; Wagner, N. J. Colloidal suspension rheology; Cambridge University Press: Cambridge, 2012
30. Zell Z. A.; Isa, L.; Ilg, P.; Leal, L. G.; Squires, T. M.; Adsorption energies of poly(ethylene oxide)-based surfactants and nanoparticles on an air-water surface. *Langmuir*. **2014**, 30, 110–119
31. Lu, J.; Bates, F. S.; Lodge, T. P. Addition of Corona Block Homopolymer Retards Chain Exchange in Solutions of Block Copolymer Micelles. *Macromolecules*. **2016**, 49, 1405-1413

32. Riess, G. Micellization of block copolymers. *Progress in Polymer Science*. **2003**, 28, 1107–1170
33. Dos Santos, S.; Medronho, B.; dos Santos, T.; Antunes, F. E. Drug Delivery Systems: Advanced Technologies Potentially Applicable in Personalised Treatment. *Advances in Predictive, Preventive and Personalised Medicine*. **2013**, 4, 35-85
34. Kabanov, A. V.; Alakhov, V. Y. Micelles of amphiphilic block copolymer as vesicles for drug delivery. In *Amphiphilic block copolymers: self assembly and applications*. Alexandridis, P.; Lindman, B.; Eds.; Elsevier: Amsterdam, 2000; pp. 347–76.
35. Bader, H.; Ringsdorf, H.; Schmidt, B. Water-soluble polymers in medicine. *Die Angewandte Makromolekulare Chemie*. **1984**, 123, 457–485
36. Caputto, A.; Betti, M.; Altavilla, G.; Bonaccorsi, A.; Boarini, C.; Marchisio, M.; Butto, S.; Sparnacci, K.; Laus, M. et al. Micellar-type complexes of tailor-made synthetic block copolymers containing the HIV-1 tat DNA for vaccine application. *Vaccine*. **2002**, 20, 2303–2317
37. Breulman, M.; Förster, S.; Antonietti, M. Mesoscopic surface patterns formed by block copolymer micelles. *Macromolecular Chemistry and Physics*. **2000**, 11, 201-204
38. Peter, P. Controlled agglomeration of latexes by block copolymers. Ph.D. Thesis. University Haute Alsace, 1998

Chapter 2

MATERIALS AND METHODS

This chapter discusses the materials and experimental methods used in investigating micelle chain exchange. Section 2.1 lists the different properties of the chosen block copolymer. An overview of different solution preparation methods is presented in Section 2.2. Section 2.3 reports the solution preparation protocol as well as the effect of dialysis and its consequent concentration determination. Section 2.4 discusses the temperature control. The control of interface is covered in section 2.5, and a more in depth explanation of the rotator is given. Lastly, a detailed discussion on dynamic light scattering (DLS) can be found in section 2.6, with a brief overview of complementary characterization techniques.

2.1 Materials

In selecting the appropriate block copolymer, a number of factors come into play. Previous work on chain exchange kinetics had been performed with poly(butadiene-*b*-ethylene oxide) (PB-PEO), giving reproducible results. More specifically, PB-PEO (1,4 isomer) has certain characteristics that are valuable for investigating chain exchange. The low glass transition temperature ($T_g = -103\text{ }^\circ\text{C}$)¹ ensures that the polymer does not exhibit glassy core dynamics at typical experimental temperatures. Additionally, a low entanglement molecular weight is expected ($M_e \sim 2\text{ kg mol}^{-1}$).² These properties are crucial to prevent interference in observing the relaxation behavior of the micelles.

To obtain spherical nanostructures the required weight fractions of the hydrophilic and hydrophobic blocks were determined consulting phase diagram specific to the polymer PB-PEO (Figure 1.1).

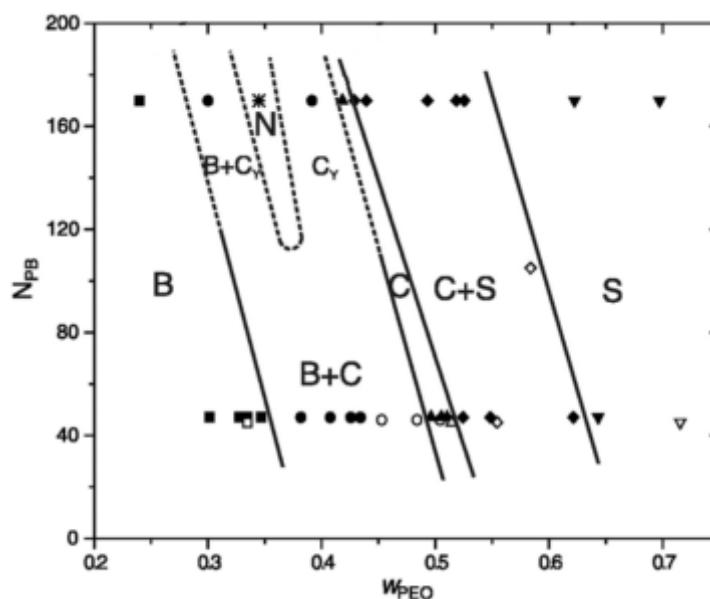


Figure 2.1: Phase diagram for dilute solutions of poly(butadiene-*b*-ethylene oxide) block polymer amphiphiles. The polymer forms various morphologies including bilayer vesicles (B), cylindrical micelles (C), spherical micelles (S), and networks (N), depending on the molecular curvature of the amphiphile. The molecular curvature is controlled by the degree of polymerization of the hydrophobic block (N_{PB}) and hydrophilic weight fraction (w_{PEO}), and the desired solution morphology can be targeted by tuning the block polymer molecular weight and composition. The figure was reproduced from Jain and Bates, *Science*, 2003, 300, 460-464. The figure was reprinted with permission from AAAS.³

Poly(1,4-butadiene-*b*-ethylene oxide) was supplied by Polymer Source (Dorval, QC, Canada) (Table 2.1).

Table 2.1: Properties of the 1,4-polybutadiene-*b*-poly(ethylene oxide) reported by Polymer Source. The molar ratios were obtained by analyzing the nuclear magnetic resonance (NMR) spectrum, with Mn the number average molecular weight and Mw the weight average molecular weight.

Mn (kg mol ⁻¹): Bd- <i>b</i> -EO	4.5- <i>b</i> -12.5
Mw/Mn (Dispersity)	1.09
Mol 1,2-PB/PEO (from ¹ H NMR)	0.026
Mol 1,4-PB/PEO (from ¹ H NMR)	0.267
Mol PB/PEO (from ¹ H NMR)	0.293

To confirm the properties of the block copolymer, the dispersity and block sizes were characterized using gel permeation chromatography (GPC) and ¹H NMR. In contrast to the data from Polymer Source, a dispersity of $D = 1.35$ was found.

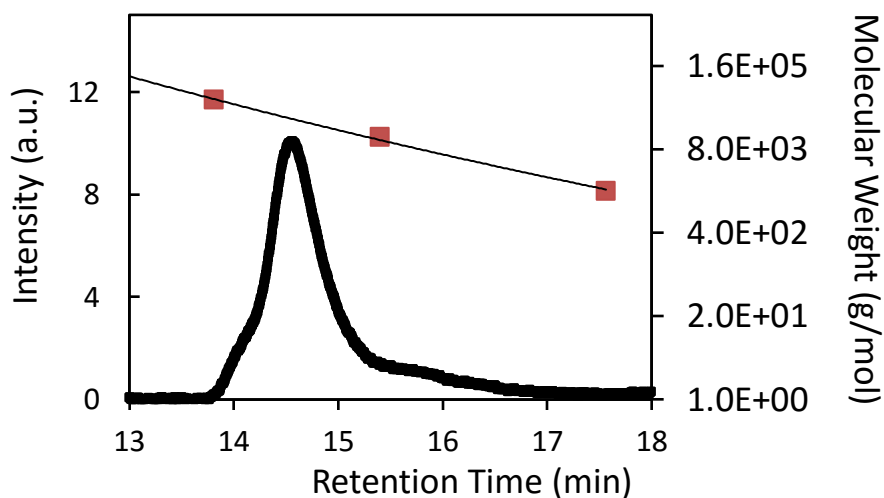


Figure 2.2: GPC spectrum of the PB-PEO sample. The retention time can be related to the molecular weight by using the linear curve.

A tail on the right side is visible, implying some residual homopolymer. The tail corresponds to the molecular weight of polybutadiene. Additionally, an NMR was run on the polymer sample to gain insight on the composition, yielding the following spectrum:

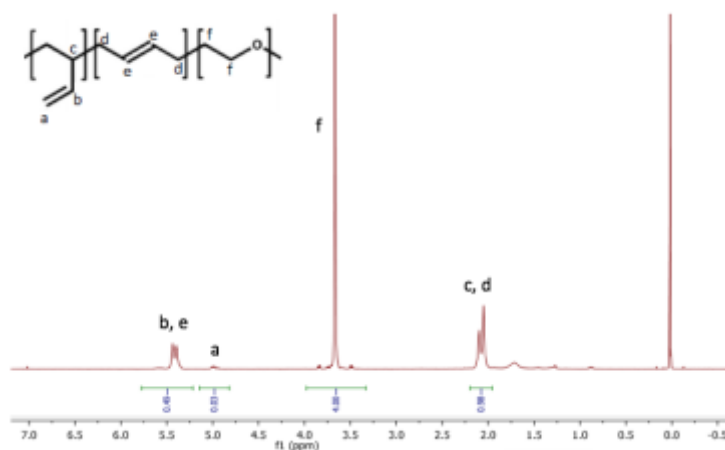


Figure 2.3: ^1H NMR spectrum obtained from the polymer sample. The different peaks are indicated with letters that correspond to molecular structures represented in the top left corner.

The different peaks represent certain chemical bonds that are characteristic to certain molecules, allowing the determination of the molar ratios of the material:

Table 2.2: Molar ratios of the PB-PEO sample determined with ^1H NMR

Mol 1,2-PB/ Mol PEO (from ^1H NMR)	0.015
Mol 1,4-PB/ Mol PEO (from ^1H NMR)	0.238
Mol PB/ Mol PEO (from ^1H NMR)	0.253

Homopolymer can not only retard chain exchange³ but also absorb into the micellar core and cause swelling. Purification of this material was thus advised before experimental use.

One possible way to remove the homopolymer is fractionation. First, the polymer was dissolved in a good solvent (tetrahydrofuran) for both the block copolymer as well as the homopolymer. The solution was then added to petroleum ether, which selectively dissolves the PB homopolymer and causes the block copolymer to precipitate. To extract as much polymer as possible, the solution was centrifuged. A yield of 71 weight% was obtained with a resulting dispersity of $\bar{D} = 1.30$. The size distribution obtained from the GPC is presented in Figure 2.4.

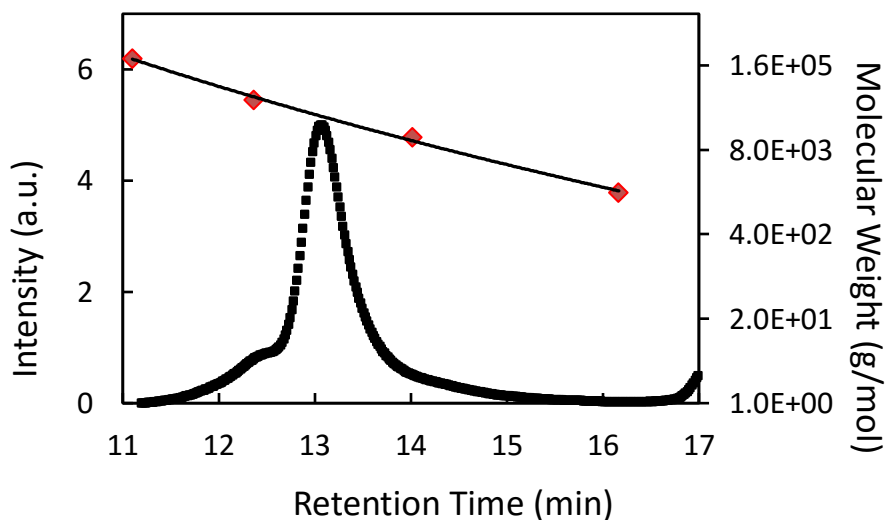


Figure 2.4: GPC spectrum of the PB-PEO sample after fractionation. The retention time can be related to the molecular weight by using the linear curve.

Whereas the right-hand tail was visibly decreased, it appears that a high molecular weight tail had developed, leading to an overall low improvement on the dispersity. A possible explanation is an increase in cross-linked polymer present in the sample. To further quantify the compositional changes, a sample was run on ^1H NMR. The spectrum and corresponding molar ratios can be found in Figure 2.5 and Table 2.3.

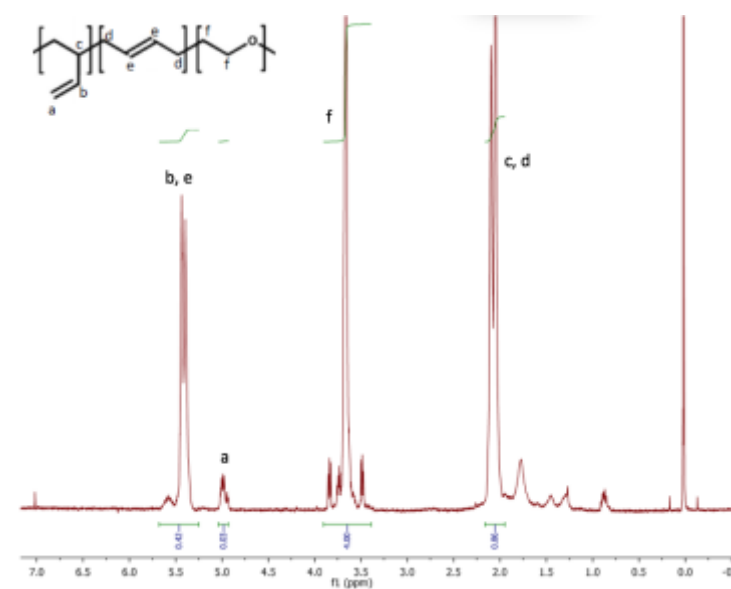


Figure 2.5: ^1H NMR spectrum obtained from the polymer sample after fractionation. The different peaks are indicated with letters that correspond to molecular structures represented in the top left corner.

Table 2.3: Molar ratios of the PB-PEO sample determined with ^1H NMR

Mol 1,2-PB/ Mol PEO (from ^1H NMR)	0.015
Mol 1,4-PB/ Mol PEO (from ^1H NMR)	0.203
Mol PB/ Mol PEO (from ^1H NMR)	0.212

The fractionation resulted in a loss of 14 mole% of 1,4-PB, while keeping the amount of PEO and 1,2-PB constant. Table 2.2 gives an overview of the different results:

Table 2.4: Properties of the polymer determined by ^1H NMR and GPC before and after fractionation. The information provided by Polymer Source is listed for comparison.

	Polymer Source	Before fractionation	After fractionation
D	1.09	1.35	1.30
$\frac{\text{mol PB}}{\text{mol PEO}}$	0.293	0.2525	0.2025

2.2 Solution methods

The characteristic features of block copolymer micelle system are largely impacted by the solution preparation methods, given the slow exchange kinetics. A number of techniques are available to produce micelles in solution. First and most straightforward is direct dissolution of micelles into a selective solvent. In general, this technique will only work if the molecular weight of the copolymer is low and the hydrophobic block is short. Prolonged stirring, temperature control and sonication can improve the solubility but are argued to lead to micelles unable to reach their equilibrium size.^{5,6}

More advanced methods include the addition and removal of cosolvents. Previous findings show the absence of micelle growth after direct dissolution in water⁷

suggesting a system in ‘near equilibrium’. To study the relaxation kinetics, cosolvent can act as a perturbation and hereby move the system away from its equilibrium. For the purpose of this thesis, tetrahydrofuran (THF) is used. THF is absorbed in the hydrophobic cores and mediates the interfacial tension between the constituent blocks, resulting in a decrease of hydrodynamic radius of the micelles.⁸ After cosolvent removal, the micelles will then grow towards their initial equilibrium position, allowing the observation of growth kinetics.

Additional methods are the emulsion method⁹ using immiscible solvents and thin-film rehydration, in which the polymer is dissolved in a good solvent, dried to form a film and then rehydrated with water.¹⁰

2.3 Preparation of micelle solutions

The fractionated polymer was dissolved in deionized water and stirred in a 20 mL scintillation glass vial with a Teflon coated cap for 3 days with a Teflon coated magnetic stirrer, at 200 rpm. Additionally, parafilm was applied to seal the cap to the glass vial. The solution was stirred at ambient temperature and pressure. Due to the photosensitivity of the polymer and to prevent crosslinking, all solutions were covered during mixing or storage. This method resulted in reproducible micelle sizes of around ~50 nm for various concentrations. In order to break up large aggregate structures, sonication was performed at 4.2 kHz for the duration of 1 h. To ensure no significant temperature changes, the sonication was split up into two intervals of 30 min between which the water and samples were allowed to cool down to room temperature.

After three days of stirring in water, tetrahydrofuran was added to obtain a polymer mixture containing 50 vol% THF in water. The solution was stirred for three more days with a Teflon coated magnetic stirrer at 200 rpm and ambient conditions in

a glass vial with a Teflon coated cap. The cap was again sealed with parafilm. This procedure has proven to give reproducible sizes, whereas if water and THF are instantaneously mixed, non-reproducible results are obtained.⁷

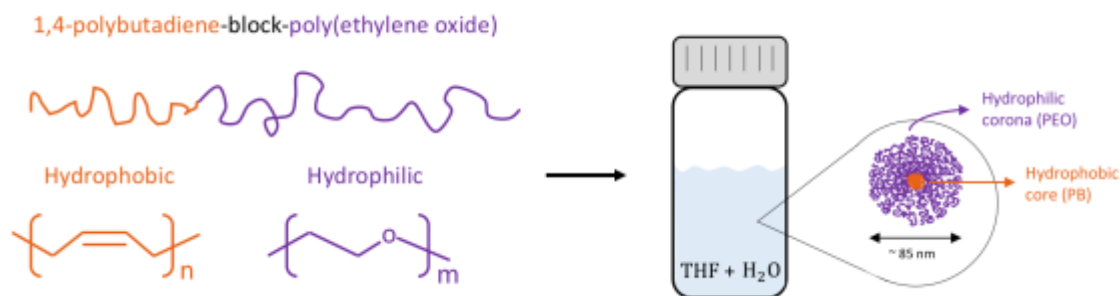


Figure 2.6: Solution preparation of the micelle solutions using the cosolvent method. After 3 days of stirring in water, THF is added. After a subsequent 3 days of stirring, dialysis is performed to remove the THF from the cores of the micelles.

Finally, the polymer solutions were dialyzed to extract THF from the cores. The dialysis tubing (Pre-treated RC Tubing 3.5 kD MWCO) was first rinsed in deionized water and soaked for 15 min. The solution was then pipetted into the tubing and clamped tight. Next, the tubing was immersed in a 200-fold excess of deionized water. This molecular weight cut-off allows THF and water to migrate but retains the polymer in the tubing, see Figure 2.7. The water was refreshed after 4 h and 8 h, with a total dialysis time of 24h. One implication of this technique is the swelling of the tube due to osmotic pressure, yielding an unknown concentration of the resulting polymer solution.

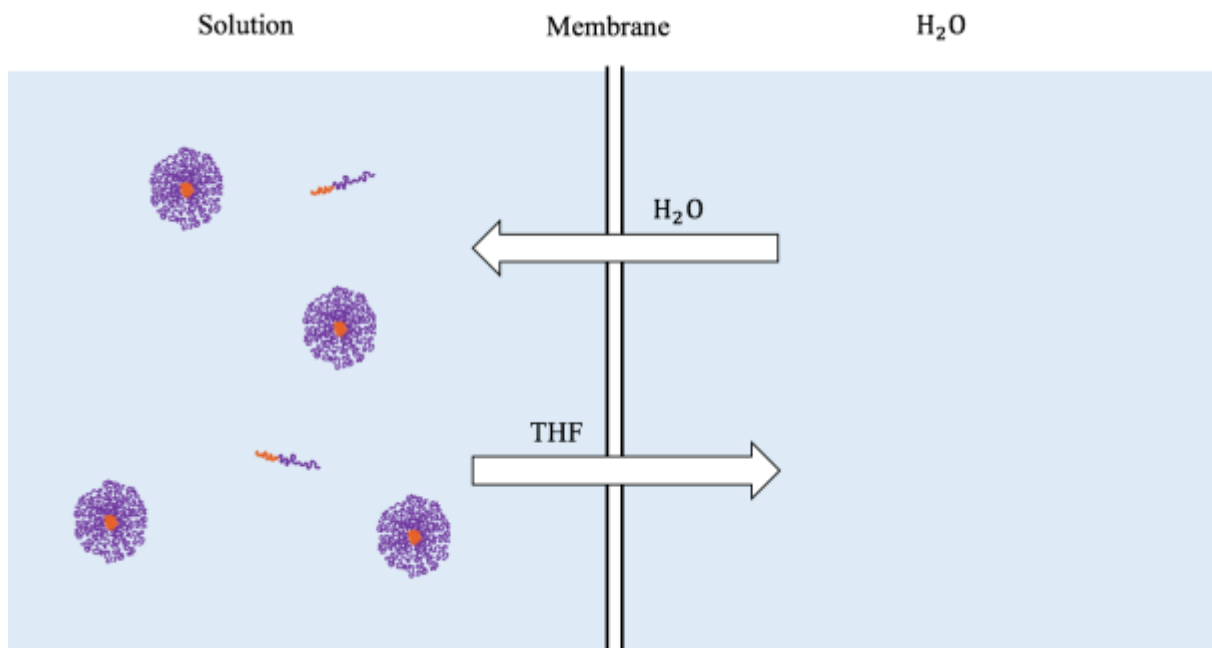


Figure 2.7: Dialysis of polymer solution with deionized water. While the polymer is not allowed to travel through the membrane, THF and water can freely interchange.

One possible way of determining concentration is using UV-Vis absorbance. From the Beer-Lambert law, a linear relation between polymer concentration and absorbance was expected and obtained, see Figure 2.8. A calibration curve was set up at a wavelength of 259 nm using the Nanodrop Spectrophotometer ND-1000. Each sample was run three times after which an average was taken.⁷ The dilution values are presented in Table 2.5.

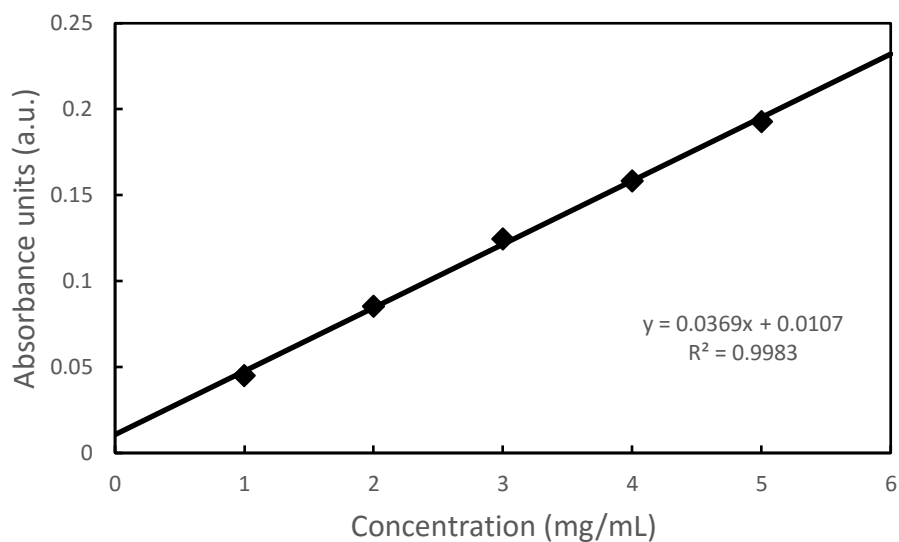


Figure 2.8: Calibration curve for PB-PEO solutions in water at $\lambda = 259\text{nm}$.

Table 2.5: Concentrations of the polymer solutions before and after dialysis.

Concentration before dialysis	Concentration post-dialysis
(mg mL⁻¹)	(mg mL⁻¹)
0.5 ± 0.1	0.3 ± 0.1
1.25 ± 0.1	0.7 ± 0.1
2.5 ± 0.1	0.7 ± 0.1

Dialysis seems to dilute the solution ~2 fold for both the 0.5 mg and 1.25 mg mL⁻¹ concentrations. However, the highest concentration yielded a dilution of almost 4-fold. This discrepancy is most likely an artifact of solution preparation but shows how this technique is susceptible to irreproducibility.

2.4 Temperature control

During storage, the block copolymer was kept refrigerated to prevent any heat induced cross-linking. The micelle solutions were magnetically stirred at ambient temperature of around ~ 23 °C. During sonication, the solutions were allowed to cool down after a 30 min interval to prevent any significant temperature changes. Similarly, solutions that were vortexed mixed were periodically stopped after each 5 min interval. During characterization using the DLS equipment, the sample was immersed in a temperature bath keeping conditions constant at 25 ± 0.1 °C.

2.5 Interface control

Methods such as vortex mixing are efficient for creating a high surface turnover rate, but lack controllability. Whereas an exact quantification is not possible, computational fluid dynamics estimate the surface turnover rate to be in the order of ~ 100 cm^2/s . A more controllable way of creating interface is using a rotator, depicted in Figure 2.9. Knowing the dimensions of the vial and the rotational speed, the amount of interface present at each position is known. The surface turnover rate can thus be accurately determined and adapted using this technique.

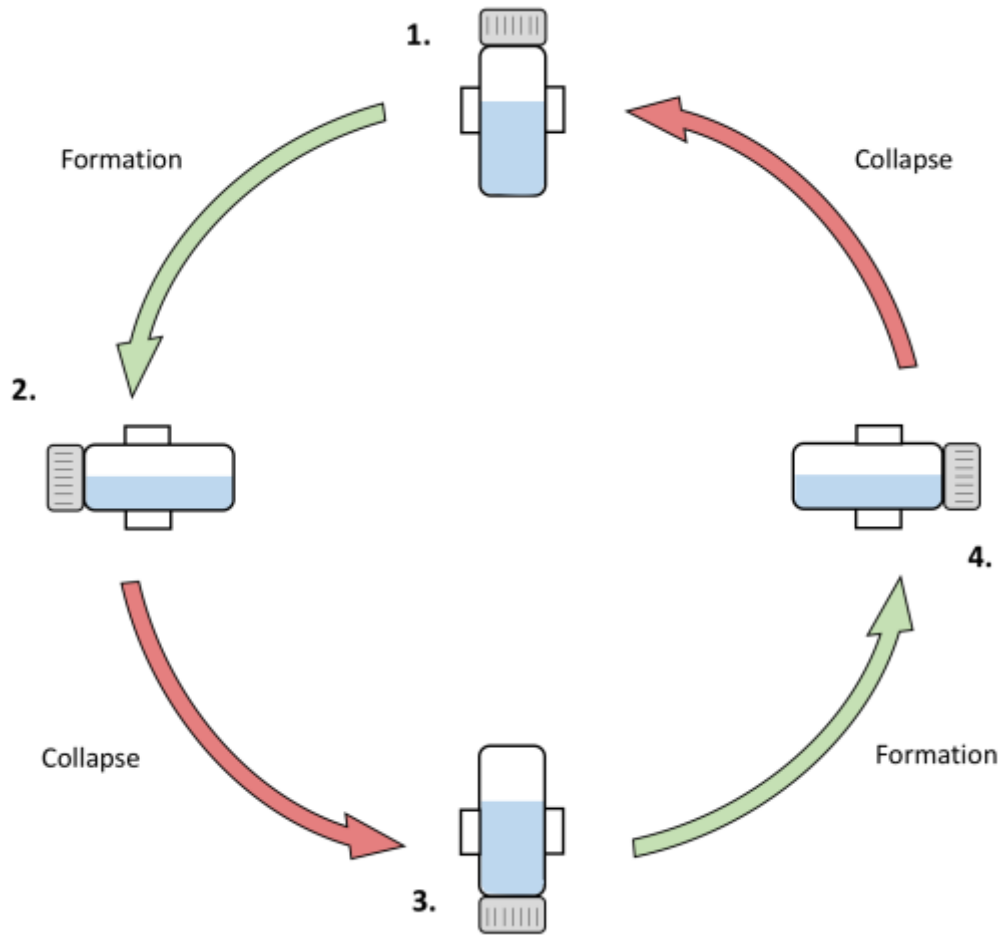


Figure 2.9: Graphical representation of the rotator device spinning counterclockwise. The green arrows indicate creation of interface whereas the red arrows represent a collapse.

Rotating in a counterclockwise manner, the samples will go from position 1 to 2, hereby creating additional interface. Upon rotating to position 3, the newly gained interface then collapses. This cycle is repeated in moving from position to 3 to 4 and back to 1. The interface is thus generated and destroyed twice in each cycle. For a cylindrical vial the highest surface turnover rate will be attained when the vial is filled halfway. When the vial is a quarter or three quarters filled, the amount of interface

generation will be identical due to symmetry but vary in interface turnover to bulk volume ratio. The rotator operates at an angular speed of 40 rounds per minute (rpm). Any higher rpm might induce centrifugal forces.

2.6 Characterization

The main focus of this thesis is to investigate chain exchange between micelles. The kinetics can be probed in multiple ways and by multiple characterization methods. The most common techniques include cryogenic transmission electron microscopy, small angle neutron scattering and dynamic light scattering. These methods are complementary and are often used concurrently. Cryogenic transmission electron microscopy (cryo-TEM) is can characterize samples without drying and provides good spatial resolution, *i.e.*, ability to examine the micelle structure. However, it lacks statistical certainty when used for quantitative analysis, is costly and requires a lot of training and overall time investment. In contrast, dynamic light scattering (DLS) offers excellent statistical certainty, is cheap in its resources as it uses light and very easy to use. The major drawback related to using this method is the poor structure resolution. A third common method is small angle neutron scattering (SANS), providing both good statistical certainty as structure resolution. Neutron scattering seems the perfect combination of DLS and cryo-TEM but comes at a very high cost. It becomes inevitable that upon characterizing nanostructures a balance between these techniques is required.

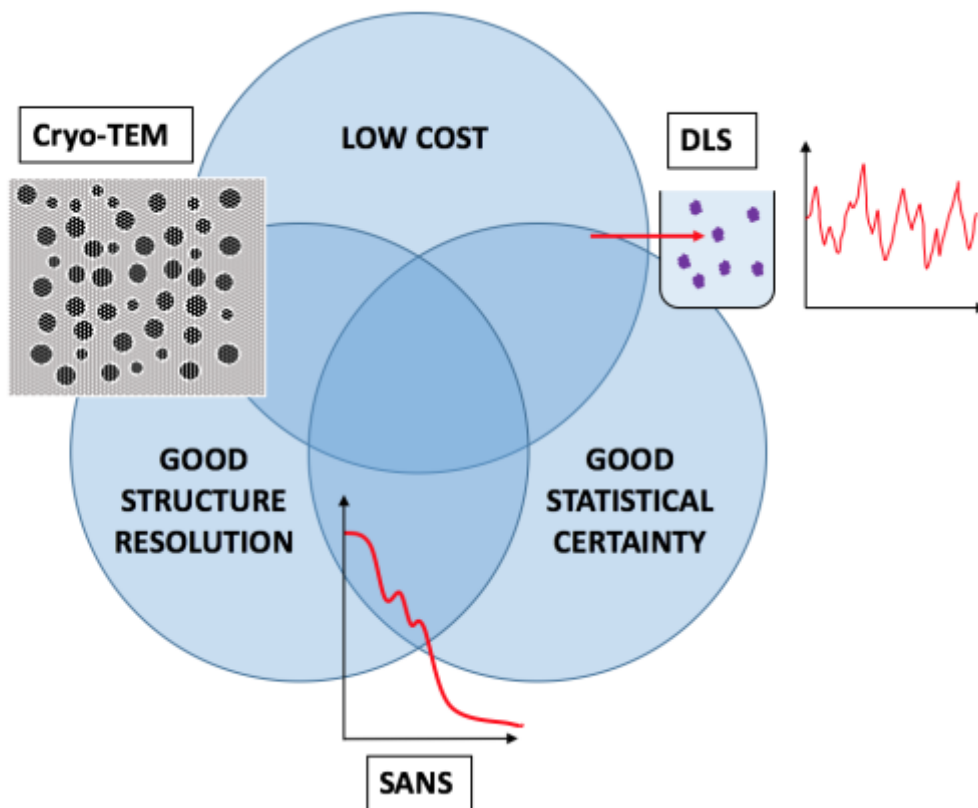


Figure 2.10: A Venn-diagram showing the advantages and disadvantages of the different characterization methods. DLS is relatively low cost and offers good statistical certainty but lacks proper structure resolution. Cryo-TEM is mid-cost and provides good structure resolution whereas DLS cannot. The drawback, however, is the poor statistical certainty when used for quantitative analysis. Lastly, SANS gives both good structure resolution and statistical certainty but comes at a high cost.

In this thesis, DLS is chosen as a primary characterization tool. Aside from the relatively low cost and fast data output, it provides useful data that can probe trends before moving on to costlier techniques. The chain exchange can be monitored by following the size evolution of the micelles. The hydrodynamic radius R_h can be extracted from dynamic light scattering using the Stokes-Einstein equation, which will

be discussed more thoroughly in section 2.6.2. While SANS and cryo-TEM could provide valuable complementary data, it is not within the scope of this work.

2.6.1 Dynamic Light Scattering

Light scattering can be divided into static light scattering (SLS) and dynamic light scattering.¹¹ Whereas SLS can determine properties such as the molecular weight M_w and R_g , DLS measurements can estimate the hydrodynamic radius R_h of nanoparticles in a solution. A major advantage of this technique is the speed at which a sample can be characterized (~3 min). Additionally, it is cheap to operate and provides good statistic certainty. An issue that is often encountered by using this method is the sensitivity of the measurement to large sized particles. As will be discussed later on, the intensity heavily scales with the radius of the particle $I \sim R^6$. This bias can result in skewed size distributions, where smaller particles are nearly undetectable in the presence of larger ones. Exceptional care must thus be taken to ensure no contamination of the sample or the DLS equipment with dust particles or fibers.

When nanoparticles are hit with light, they will scatter in different directions. The scattering intensity will fluctuate over time, as the particles are in constant movement due to Brownian motion. This variation in intensity can therefore be related to the kinetic properties of the particles and yield their diffusion coefficients. Larger particles will have a smaller diffusivity and less fluctuation in intensity with respect to smaller particles, see Figure 2.11:

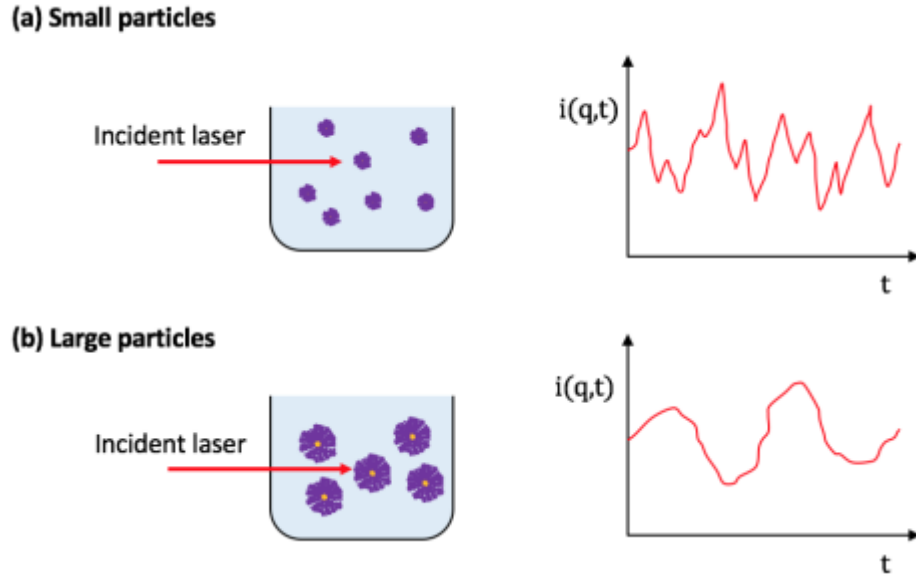


Figure 2.11: DLS on micelle solutions with as output a more fluctuation intensity for smaller particles (a) with respect to larger particles (b)

The scattering wave vector \mathbf{q} can be defined as the difference between scattered and incident wave vectors, with a magnitude q :¹²

$$q = \frac{4\pi n_r}{\lambda} \sin\left(\frac{\theta}{2}\right) \quad (2.1)$$

with λ the wavelength of the laser, n the refractive index of the solvent and θ the angle at which the intensity is measured. For the setup used in this thesis ($\lambda = 532 \text{ nm}$, $n_r = 1.336$ and $\theta = 90^\circ$) yielding $q \sim 0.00223 \text{ \AA}^{-1}$.

During the DLS experiment, the intensity is measured over a period of time t_f . As could be seen in Figure 2.11, the fluctuation of the intensity seems to be random around and average value. A logical conclusion considering it is the result of the random Brownian motion. This average intensity can be written as:¹¹

$$i_{av} = \lim_{t_f \rightarrow \infty} \frac{1}{t_f} \int_0^{t_f} i(q, t) dt \quad (2.2)$$

The deviation from this average value is what gives us a quantification of the variance in intensity and can be characterized with the autocorrelation function:

$$g(q, \tau) = \lim_{t_f \rightarrow \infty} \frac{1}{t_f} \int_0^{t_f} i(q, t) i(q, t + \tau) dt \quad (2.3)$$

with τ the delay time between two signals. In reality, the intensity is measured in n discrete time steps with $t_f = n\Delta t$. The autocorrelation function correlates the intensity at a certain point in time t , to the intensity at a time $t + \tau$. Intuitively one can see that a smaller delay time corresponds to a higher correlation. Conversely, for a delay time $\tau \rightarrow \infty$, the intensities will become uncorrelated and independent of τ . The autocorrelation function $g(q, \tau)$ should thus decrease with increasing τ . Normalizing the correlation function to the uncorrelated value obtained at τ_∞ yields the Siegert relation:

$$g^2(q, \tau) = 1 + A|g^1(q, \tau)|^2 \quad (2.4)$$

with A a constant that is approximately ~ 1 . DLS instruments typically come with a software that provides the function $g^1(q, \tau)$. However, the raw data can also be extracted and manually fit using programs such as MATLAB, IGOR Pro or ORIGINS Pro, allowing more controllability and processability of the results. For this thesis, MATLAB is used to process the autocorrelation data gained from the DLS equipment.

2.6.2 Fitting the correlation function

The autocorrelation data can be fit to different functions. Three prominent methods will be discussed here: the quadratic cumulant (QC) method, the double exponential (DE) and the polydisperse double exponential (PDE).

One of the most common fits for correlation data is the cumulant method.¹³ The exponential decay of the correlation function is valid for monodisperse particles.

It can characterize both the average size of the micelles as their polydispersity. The cumulant fit can be written as:

$$|g^1(q, \tau)| = C_1 \exp\left(-\Gamma\left(\tau + \frac{\mu_2}{2!} \tau^2 + \frac{\mu_3}{3!} \tau^3 + \dots\right)\right) \quad (2.5)$$

With C_1 a coefficient, Γ the average decay rate, Γ/μ^2 the second order polydispersity index, the wave vector magnitude q , and the delay time τ . Using the relation $\Gamma = q^2 D$, with D the diffusion coefficient and neglecting any terms higher than second order, the quadratic cumulant fit is obtained:¹⁴

$$|g^1(q, \tau)| = C_1 \exp(-q^2 D \tau) \left(1 + \frac{\mu}{2} \tau^2\right) \quad (2.6)$$

where the polydispersity coefficient $\sigma = \mu/(q^2 D)^2$ gives the size distribution of the population. It is advised to use this method for a small τ and to not use terms with orders higher than τ^3 , as they can lead to overfitting.¹⁵ A major advantage of this technique is its insensitivity to noise.

A second technique to fit the intensity decay rate is the double exponential fit, which can be written as follows:

$$g^1(q, \tau) = C_1 \exp(-q^2 D_1 \tau) + C_2 \exp(-q^2 D_2 \tau) \quad (2.7)$$

From this fit, two distinct particle sizes can be obtained. This method is thus very useful for bimodal distributions. A possible extension of this method uses the polydispersity coefficient that are also used in the QC, obtaining the polydisperse double exponential:

$$g^1(q, \tau) = C_1 \exp(-q^2 D_1 \tau) \left(1 + \frac{\mu_1}{2} \tau^2\right) + C_2 \exp(-q^2 D_2 \tau) \left(1 + \frac{\mu_2}{2} \tau^2\right) \quad (2.8)$$

In addition to characterizing two nanoparticle sizes, the PDE yields two polydispersity coefficients for the respective sizes.

From these fits, the diffusion coefficient is obtained for either one or two sizes. The Stokes-Einstein equation can then be used to retrieve the hydrodynamic radius of the particle:

$$D = \frac{k_B T}{6\pi\eta R_h} \quad (2.9)$$

with k_B the Boltzmann constant, T the temperature and η the dynamic viscosity of the solution. Acquiring the particle size is the most common use of DLS but is sometimes also used to obtain the viscosity.¹¹

2.6.3 Equipment and procedures

The dynamic light scattering experiments were performed on the Brookhaven Instrument Light Scattering System (BI-200SM, Brookhaven Instruments Corporation, BIC) equipped with a CNI Laser (532 nm). The angle of the detector was kept constant at 90° for all experiments. The sample was contained in cylindrical Kimble 15x45 mm 1 dram vials and directly placed inside the sample holder. The decalin bath was filtered for ~10 min before use and all samples and holders were sprayed with dust remover to make sure no dust particles would interfere. The count rate was kept in the range of 50-500 kcps. Before taking measurements, the samples were allowed to reach the temperature of the bath, set at 25.0 ± 0.1°C. During measurements, the count rate history was also checked to ensure no sudden jumps, which could indicate the presence of dust. The correlation data was then extracted from the BIC software and manually fit in MATLAB.

REFERENCES

1. Kanaya, T.; Kawaguchi, T.; Kawi, K. Local dynamics of cis-1, 4-polybutadiene near the glass transition temperature T_g . *Physica B: Condensed Matter*. **1992**, 182, 403-408
2. Roovers, J. Linear Viscoelastic Properties of Polybutadiene. A Comparison With Molecular Theories. *Polymer Journal*. **1986**, 18, 153-162
3. Jain, S.; Bates, F. On the origins of morphological complexity in block copolymer surfactants. *Science*, **2003**, 300, 460-464
4. Lu, J.; Bates, F. S.; Lodge, T. P. Addition of Corona Block Homopolymer Retards Chain Exchange in Solutions of Block Copolymer Micelles. *Macromolecules*. **2016**, 49, 1405-1413
5. Gohy, J.F. Block Copolymer Micelles. *Advances in Polymer Science*. **2005**, 190, 65-136
6. Karayianni, M.; Pispas, S. Self-Assembly of Amphiphilic Block Copolymers in Selective Solvents. In Fluorescence Studies of Polymer Containing Systems. Karayianni, M.; Pispas, S.; Eds.; Procházka, K., 2016; pp 24-64
7. Kelley, E. G.; Murphy, R. P.; Sepalla, J. E.; Smart, T. P.; Hann, S. D.; Sullivan, M. O.; Epps, T. H. Size evolution of highly amphiphilic macromolecular solution assemblies via a distinct bimodal pathway. *Nature Communications*. **2014**, 5, 3599
8. Murphy, R. P.; Kelley, E. G.; Rogers, S. A.; Sullivan, M. O.; Epps, T.H. Unlocking Chain Exchange in Highly Amphiphilic Block Polymer Micellar Systems: Influence of Agitation. *ACS Macro Letters*. **2014**, 3, 1106-1111
9. Zhu, J.; Hayward, R. C. Spontaneous Generation of Amphiphilic Block Copolymer Micelles with Multiple Morphologies through Interfacial Instabilities. *Journal of the American Chemical Society*. **2008**, 130, 7496-7502

10. Liu, J.; Lee, H.; Allen, C. Formulation of drugs in block copolymer micelles: drug loading and release. *Current Pharmaceutical Design*. **2006**, 12, 4685–701
11. Hiemenz, P. C.; Rajagopalan, R. Principles of colloid and surface chemistry, 3rd ed.; Eds.; CRC/Taylor & Francis: Boca Raton, FL, 1997
12. Frisken, B. J. Revisiting the Method of Cumulants for the Analysis of Dynamic Light-Scattering Data. *Applied Optics*. **2001**, 40, 4087–4091
13. Koppel, D. E. Analysis of Macromolecular Polydispersity in Intensity Correlation Spectroscopy: The Method of Cumulants". *The Journal of Chemical Physics*. **1972**, 57, 4814
14. Hassan, P.; Kulshreshtha, S. Modification to the cumulant analysis of polydispersity in quasielastic light scattering data. *Journal of colloid and interface science*. **2006**, 300, 744–748
15. Chu, B. Laser Light scattering: Basic Principles and Practice, 2nd ed. Eds.; Academic Press. 1992

Chapter 3

RESULTS AND DISCUSSION

The focus of this thesis is to investigate the growth mechanisms at work in block copolymer micelles, more specifically the influence of the air-water interface. The size evolution of micelles was probed over time under varying conditions using dynamic light scattering. The autocorrelation data obtained from the DLS software was extracted from the BIC software and manually fit using MATLAB. The relaxation kinetics of the micelles can be examined by perturbing the system from its equilibrium using the cosolvent method (3.1). Upon removal of the solvent, the micelles will then grow towards their new equilibrium size through multiple fusion events. This micellar growth is characterized by a bimodal distribution (3.2).

Building on the hypothesis of an interface mediated growth, the interface turnover rate to bulk volume ratio was varied in experiments using both the vortex mixer and rotator (3.3.1). Whereas vortex mixing creates more interface over time, the rotator allows for more controllability and a better quantification. Vortex mixing the solutions resulted in a clear difference in micelle chain exchange. Vials with less bulk volume created more air-water contact, resulting in a faster growth. Rotating the samples resulted in a less pronounced effect, with a small distinction between vials that were filled for 25% and 50% with respect to the 75%. An additional experiment characterized the influence of the concentration on the growth kinetics (3.3.2). Zero-order kinetics, *i.e.*, micelles growing equally fast for different concentrations, would suggest interfacial nucleation. The two concentrations that were examined over time

varied in initial conditions but appeared to grow equally fast until their equilibrium size was reached.

3.1 Cosolvent method

The pathway dependency of block copolymer micelles highlights the importance of solution preparation on the micellar properties. Methods such as direct dissolution, thin-film rehydration and the cosolvent method are known to lead to vastly different micelle sizes.¹ It is also important to note that the effects of different methods are dependent on the block copolymers being used.

The cosolvent method is used here as a means to probe relaxation kinetics. The protocol was discussed in detail in section 2.3 but will briefly be revisited. The polymer was dissolved in aqueous solvent and stirred for 3 days while being covered to prohibit any light induced cross-linking. THF was added to the solution after which the mixture was stirred for a consecutive 3 days. In order to extract THF from the micellar cores, dialysis was performed over a total period of 24 h. Day 0 indicates the day at which dialysis was finished and the solution has not yet been agitated. After the addition and removal of THF, the micelles decreased in size, see Table 3.1 and Figure 3.1.

Table 3.1: The hydrodynamic radius D_h and polydispersity σ for direct dissolution and the cosolvent method. The hydrodynamic radius of the micelles decreased upon addition and removal of cosolvent.

	D_h (nm)	σ
Direct dissolution	44.79 ± 0.76	0.17 ± 0.01
Cosolvent method	20.6 ± 0.35	0.19 ± 0.04

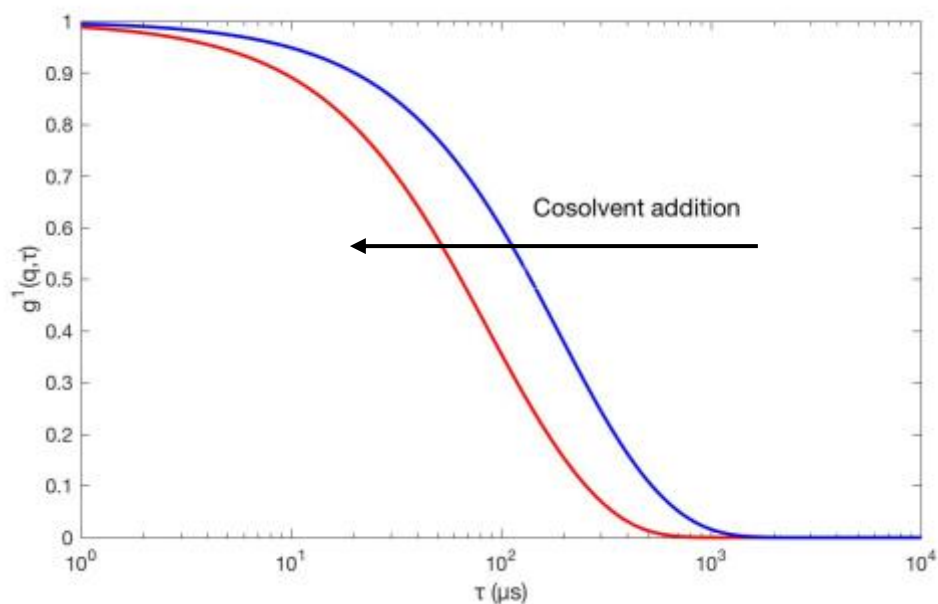


Figure 3.1: Autocorrelation functions for the cosolvent method (red) and direct dissolution (blue) using the quadratic cumulant fit in MATLAB. Note that the autocorrelation data were normalized for ease of comparison. The larger size of the micelles present in the direct dissolution sample corresponds to a delayed exponential decay.

The reduction in hydrodynamic radius was expected given the decrease in interfacial tension induced by the cosolvent. Subjecting the solution to vortex mixing caused the hydrodynamic radius to increase, indicating chain exchange. The DLS data showing this size evolution over time are provided in Figure 3.2.

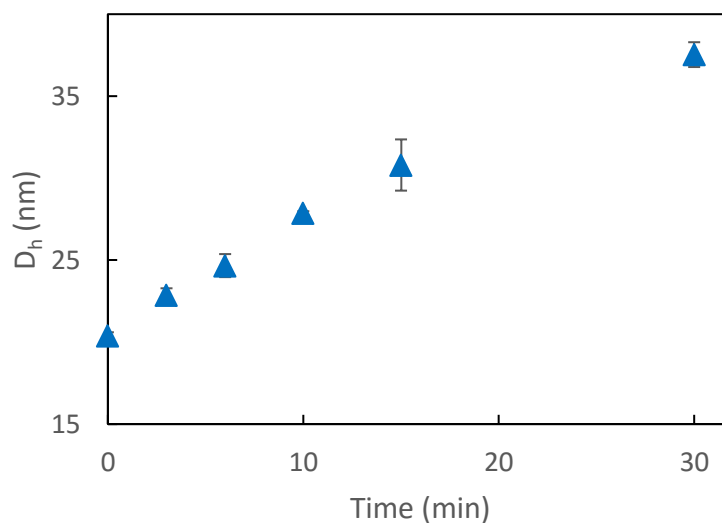


Figure 3.2: Size evolution of a 2.5 mg mL⁻¹ PB-PEO sample after dialysis. The solution was vortex mixed for 30 minutes. The error bars were obtained by taking triplicate DLS measurements of the sample.

The micelles appear to grow linearly as a function of time towards the equilibrium size of 42 nm previously obtained for direct dissolution. The sizes that are represented on this graph, however, are an average and not representative of the actual micelle sizes. The micelles are indeed growing, but rather than slowly shifting from one size to another, the micelle population contains a bimodal distribution. The next section discusses this in further detail.

3.2 Bimodal size distribution

The growth of micelles is usually attributed to two main mechanisms: fusion/fission or single chain exchange (see section 1.4). While numerous papers report the prevalence of single chain exchange,^{2,3} others argue the importance of micelle fusion and fission.⁴ The actual mechanisms at hand still remain mostly unresolved.

Cryo-TEM images of PB-PEO micelles system perturbed far away from their equilibrium have demonstrated the appearance of a distinct bimodal distribution upon growth.¹ Over time the two sizes in this distribution stayed constant but changed in proportion. Starting off with exclusively micelles of size D_{h1} and polydispersity σ_1 , the population increased in percentage of micelles of the larger size D_{h2} . Eventually, the solution reached a state in which only micelles of size D_{h2} were present. A stepwise fusion based growth would lead to a multimodal distribution and does not agree with these findings. Alternatively, single-chain exchange would lead to a monomodal shift in micelle size and also offers no explanation, leading to the hypothesis that the PB-PEO micelles grow through some alternate fusion based mechanism with a bimodal pathway.

The sizes in Figure 3.2 were obtained using the quadratic cumulant fit, which assumes a monodisperse distribution. Using this method, the hydrodynamic diameter and polydispersity coefficient were allowed to vary. A polydisperse double exponential method was also investigated to fit the decay rate of the autocorrelation data with two fixed sizes $D_{h1} = 20.4 \text{ nm}$ and $D_{h2} = 42 \text{ nm}$. These sizes were determined by the initial and final diameters of the micelles, assuming that micelles of these sizes make up the populations of the systems. The fitted parameters were the weights for the exponential terms C_1 and C_2 , which are normalized so that $C_1 + C_2 =$

1, and the polydispersities σ_1 and σ_2 . Figure 3.4 compares the fits that were obtained using the QC and PDE.

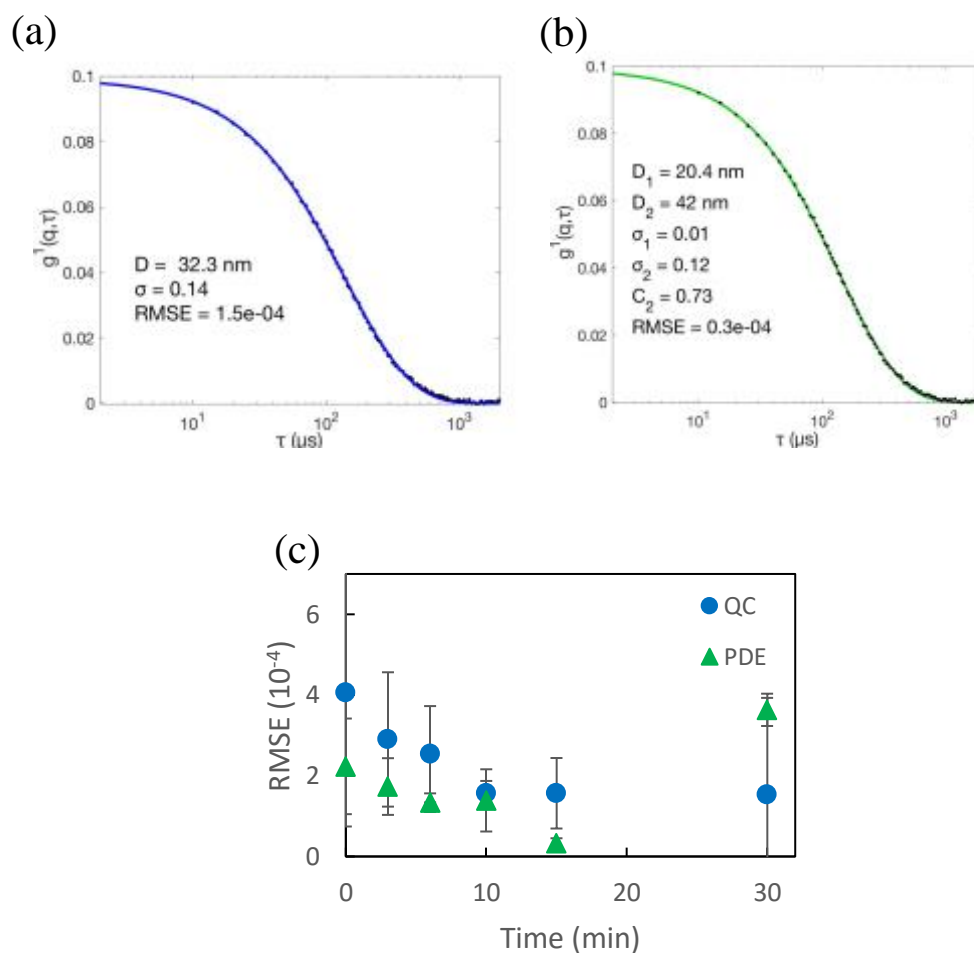


Figure 3.3: The autocorrelation data of a 2.5 mg mL^{-1} PB-PEO sample that was vortex mixed for 15 minutes with the QC (a) and the polydisperse double exponential (b). The RMSE for both methods over a time period of 30 minutes is given in (c). The error bars represent the standard deviation obtained by taking triplicate DLS measurements of the sample.

Both methods seem to fit the data almost identically, demonstrating the plausibility of the bimodal size distribution. Additional evidence can be gained by performing cryo-TEM and SANS.¹ It is also important to note the sensitivity of the light scattering experiment to larger sizes. Knowing that the intensity scales as $I \sim R^6$, size distributions can be skewed, where smaller particles can be hardly detected in the presence of larger ones. Therefore, DLS is not suited for exact kinetic models but rather is more useful for qualitative analysis. Figure 3.5 (a) shows how the intensity weight coefficient C_2 , *i.e.*, for the large size, varies over time and Figure 3.5 (b) gives the corresponding polydispersity for the two sizes.

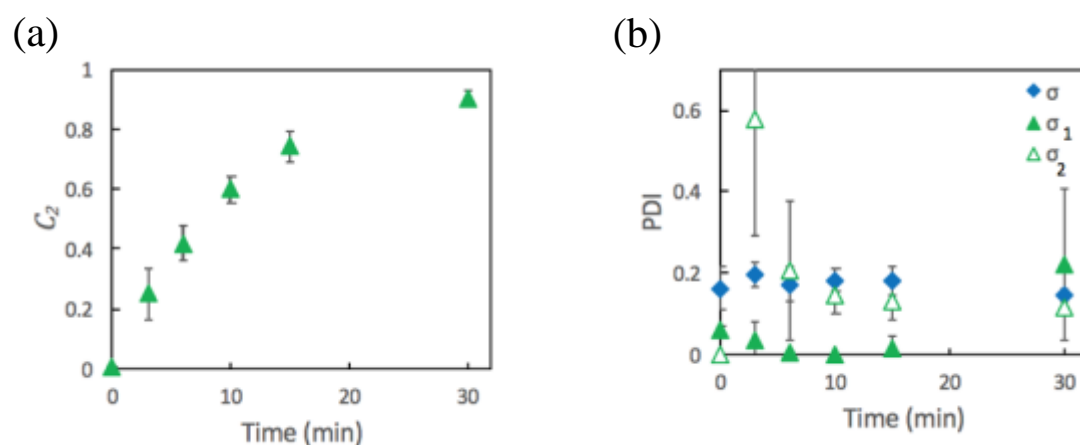


Figure 3.4: The change of the intensity weight coefficient C_2 over time for a 2.5 mg mL⁻¹ sample being vortex mixed for 30 minutes (a). The corresponding polydispersities of the two populations σ_1 and σ_2 along with the polydispersity obtained from the QC are given in (b). The error bars represent the standard deviation obtained by taking triplicate DLS measurements of the sample.

The intensity weight coefficient C_2 shows an initial fast growth rate that flattens out as it nears the plateau. Intuitively, this type of behavior is expected. As

time increases, fewer of the smaller sized micelles will be present to fuse together. The rate of chain exchange should thus decrease over time.

3.3 Interface mediated micelle growth

Adsorption of nanoparticles to the interface has been used in a variety of applications and is often found to be irreversible.^{6,7} Techniques such as vortex mixing can deform the interface and mediate the adsorption and desorption of the micelles. The effect of interfacial nucleation can be probed by multiple experiments. First the bulk volume to interface turnover rate is varied (3.3.1). If the interface is indeed the rate limiting factor, a higher interface turnover rate per bulk should yield a faster growth. This experiment is performed using both vortex mixing and rotating. Additionally, the influence of the concentration on micelle growth is investigated (3.3.2). The hypothesis of interfacial nucleation dictates no dependency on concentration *i.e.*, a zero-order kinetics.

3.3.1 Varying bulk to interface turnover rate

Three vials filled up to varying extents were vortex mixed for 30 minutes with micelle size analyses performed at 3, 6, 10 and 15 minutes. The high surface turnover rate was expected to equilibrate the micellar systems in a matter of minutes. The size evolution can be plotted using the intensity weight C_2 obtained from the polydisperse double exponential fit, with $D_{h1} = 20.4 \text{ nm}$ and $D_{h2} = 42 \text{ nm}$:

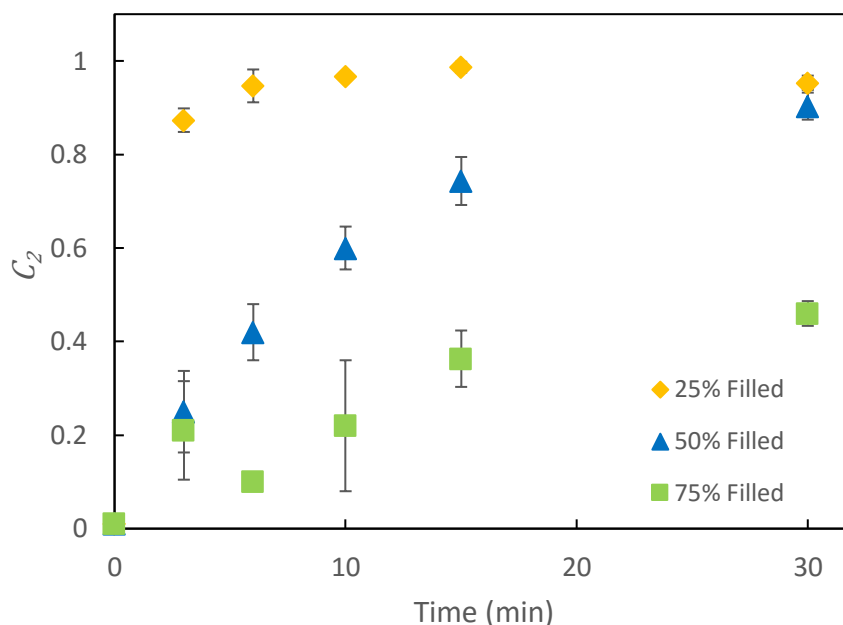


Figure 3.5: Micelle size evolution for samples with 25% filled vials (yellow diamonds), 50% filled vials (blue triangles) and 75% filled vials (green squares), with C_2 the intensity weight coefficient obtained from the PDE fit. The samples were vortex mixed for 30 min total. The error bars were obtained by taking triplicate DLS measurements of the sample. Note that the error bars are sometimes smaller than the marker size and therefore not always visible.

The 25% filled vial quickly grew towards its final micelle size, vastly outpacing the other samples. The plateau occurred after ~10 min of vortex mixing. Both the lower bulk volume as the potential for a more air-water contact during vortex formation contributed to this result. The 50% filled vial follows a slower trend towards its equilibrium, suggesting a difference in chain exchange rate. The 75% filled vial strongly lags behind the other two samples, and was nowhere near its equilibrium size even after 30 minutes of vortex mixing. The limited amount of air present in this sample led to a low surface turnover rate that was visually noticeable during the

experiment. Whereas the first sample created a vortex with an air-water interface that spanned almost the entire vial, the size of the vortex decreased drastically for the 50% and 75% filled vials. The results agree with the hypothesis of interfacial nucleation as a kinetic pathway for block copolymer micelles. All solutions were subjected to the same amount of shear flow but to a varying interface turnover rate.

The experiment was repeated using a rotator device. Even though the surface turnover rate for vortex mixing is expected to be an order of magnitude higher, the rotator allows for an exact quantification. The dimensions of the vial are given in Figure 3.6, with the surface turnover rates and their respective ratio to bulk presented in Table 3.2.

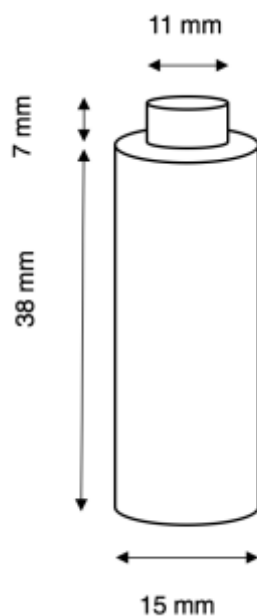


Figure 3.6: Dimensions of the vial. Note that the thickness of the vial (= 1 mm) has to be taken into account upon calculating the surface turnover rate.

Table 3.2: The surface turnover rates and their respective ratio to the bulk for vials filled 25%, 50% or 75%.

	Surface turnover rate ($\text{cm}^2 \text{s}^{-1}$)	Turnover rate per bulk ($\text{cm}^2 \text{mL}^{-1} \text{s}^{-1}$)
25 % filled	6.7	5.4
50 % filled	8.1	3.3
75 % filled	6.7	1.8

Interesting here is that unlike the vortex mixer, the 25% and 75% filled vials create the same amount of surface turnover but vary in their ratio to bulk volume. In contrast to the previous findings, the two micelle populations present in this experiment are $D_{h1} = 34 \text{ nm}$ and $D_{h2} = 53 \text{ nm}$. The difference in initial size is most likely an artifact of the solution preparation. Depending on how far a micellar system is perturbed away from its equilibrium size, different ‘near equilibrium’ states can be reached,¹ which could potentially explain the discrepancy in final micelle size. It is, however, counterintuitive that the vortex mixed solutions attained a lower final micelle size with respect to the rotated samples. The size evolutions that correspond to these samples are given in Figure 3.7 using the PDE fit.

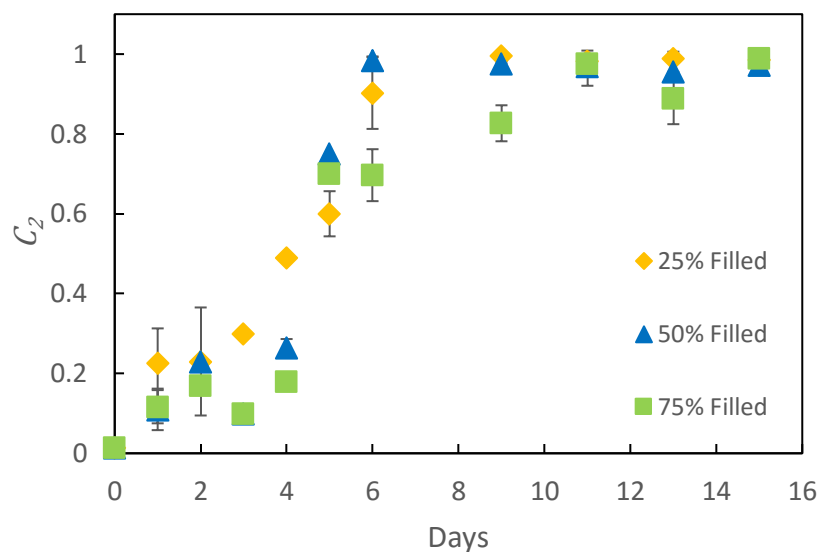


Figure 3.7: Micelle size evolution for samples with 25% filled vials (yellow diamonds), 50% filled vials (blue triangles) and 75% filled vials (green squares), with C_2 the intensity weight coefficient obtained from the PDE fit. The samples were rotated at 40 rpm. The error bars represent the standard deviation obtained by taking triplicate DLS measurements of the sample. Note that the error bars are sometimes smaller than the marker size and therefore not always visible.

With respect to the vortex mixing experiment, the difference in micelle growth was hardly noticeable. The 25% and 50% filled reach their plateau around day 6. The 75% filled follows the behavior of the other two samples up to day 6, where it seems to flatten out, reaching its equilibrium size at day 12. Interestingly, these samples do not seem to exhibit an initially fast growth that decays over time, as was seen in Figure 3.5. Even though the surface turnover rates vary substantially, the micellar growth hardly seems impacted. A possible explanation for these results is that the turnover rates are not high enough for a significant amount of interfacial nucleation to occur. The difference in turnover rates would then hardly matter. Additionally, the lack of

micelle growth can be allocated to the limited amount of surface ruptures. Whereas the air-water interface is continuously subjected to a high shear rate during vortex mixing, the shear rates inherent to the rotator might not be sufficient.

To put these timescales in perspective, the relaxation times using the rotator seem to lie somewhere in between a vortex mixer and a magnetic stirrer. Where the former can equilibrate micelle systems in half an hour or less, the latter can take up to weeks to reach its equilibrium size.¹

The results from this experiment are not conclusive as the noise on the data gathered from the DLS and the low surface turnover rates led to no significant difference between the samples. Even after processing the autocorrelation data and fits, the output was hardly smoothed. Samples with a larger difference in surface turnover rate per bulk volume might lead to a more pronounced difference.

3.3.2 Varying concentration

In addition to varying interface turnover ratios, the effects of varying concentrations were evaluated as a complementary experiment to investigate interfacial nucleation. Zero-order kinetics have been found in previous work using vortex experiments.⁵ However, it is hard to know whether different samples were equally agitated using this technique. For this reason, the rotator was used over a period of 10 days to examine the concentration dependency of the growth kinetics. For 0.5 mg/mL an initial size of $D_{h1} = 28$ nm was found and for 1.25 mg/mL, $D_{h1} = 20.4$ nm was obtained. In the future, this difference as a solution preparation artifact can be avoided by diluting samples from one mutual batch. Both samples, however, equilibrated at the same micelle size of $D_{h2} = 53$ nm. Figure 3.8 shows the size evolution:

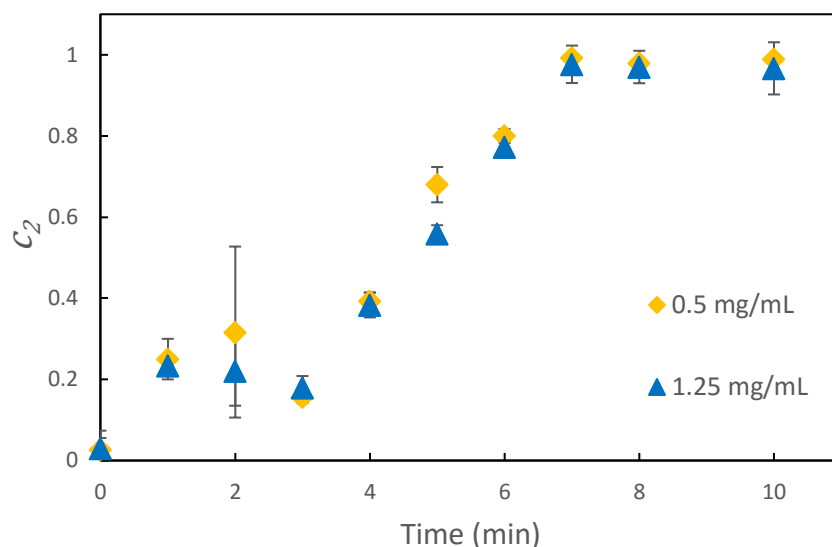


Figure 3.8: Micelle size evolution for samples with 0.5 mg mL^{-1} (yellow diamonds) and 1.25 mg mL^{-1} (blue triangles), with C_2 the intensity weight coefficient obtained from the PDE fit. The error bars were obtained by taking triplicate DLS measurements of the sample. Note that the error bars are sometimes smaller than the marker size and therefore not always visible.

The micellar growth shows a similar trend to Figure 3.7. Both concentrations appear to grow equally fast, suggesting an interface-limited chain exchange. A fusion/fission based growth would show a second-order rate kinetics, in contrast to the obtained zero-order. Even though this seems to agree with the hypothesis, it can be argued that due to the low surface turnover rates inherent to the rotator, differences in chain exchange are possibly not unlocked. Nonetheless, this result agrees with the proposed role of the interface as a mediator for chain exchange.

REFERENCES

1. Kelley, E. G.; Murphy, R. P.; Sepalla, J. E.; Smart, T. P.; Hann, S. D.; Sullivan, M. O.; Epps, T. H. Size evolution of highly amphiphilic macromolecular solution assemblies via a distinct bimodal pathway. *Nature Communications*. **2014**, *5*, 3599
2. Halperin, A. Polymeric Micelles: A Star Model. *Macromolecules*. **1987**, *20*, 2943-2946
3. Prhashanna, A.; Khan, S. A.; Chen, S. B. Kinetics of Chain Exchange between Diblock Copolymer Micelles. *Macromolecular Theory and Simulations*. **2016**, *25*, 383-391
4. Dormidontova, E. E. Micellization kinetics in block copolymer solutions: scaling model. *Macromolecules*, **1999**, *32*, 7630–7644
5. Murphy, R. P.; Kelley, E. G.; Rogers, S. A.; Sullivan, M. O.; Epps, T. H. Unlocking Chain Exchange in Highly Amphiphilic Block Polymer Micellar Systems: Influence of Agitation. *ACS Macro Letters*. **2014**, *3*, 1106-1111
6. Zell Z. A.; Isa, L.; Ilg, P.; Leal, L. G.; Squires, T. M. Adsorption energies of poly(ethylene oxide)-based surfactants and nanoparticles on an air-water surface. *Langmuir*. **2014**, *30*, 110–119
7. Riess, G. Micellization of block copolymers. *Progress in Polymer Science*. **2003**, *28*, 1107–1170

Chapter 4

THESIS OVERVIEW AND FUTURE RECOMMENDATIONS

4.1 Conclusion

In expanding the knowledge of block copolymer micelles and their behavior, development and optimization of new applications can emerge. Despite being used in a wide range of fields, the fundamental growth mechanisms at work remain mostly unresolved. This thesis focuses on probing the influence of the interface on the kinetic pathway of the micelles. In doing so, dynamic light scattering is chosen as a primary characterization tool to monitor the micelle sizes over time.

Chapter 2 reported the properties of the block copolymer of use, as well as its subsequent purification. Additionally, solution preparation methods were discussed including the concentration determination of post-dialysis solutions. Moreover, an overview of different characterization methods was given, with an in-depth discussion of Dynamic Light Scattering (DLS).

The results reported in Chapter 3 demonstrated the influence of cosolvent addition on the micelle size and its use for perturbing the micellar system. After dialyzing tetrahydrofuran (THF) out of the cores, the micelles grew to their new equilibrium size. The autocorrelation data was fit using the quadratic cumulant (QC), showing a gradual shift in micelle sizes until a plateau was reached. Additionally, the polydisperse double exponential (PDE) was shown to fit equally well, supporting the hypothesis of growth through a bimodal pathway. The relationship between micellar growth and the air-water interface was probed by characterizing samples with varying

interface turnover rate to bulk volume ratios. Vortex mixing the samples showed how different filling levels of vials largely influenced the chain exchange rate, suggesting an interface mediated growth mechanism. Additionally, the same experiment was repeated on a rotator. A less pronounced difference was obtained, where only the 75% filled vial showed a growth rate that was distinguishably slower than the others. Overall, the data for this experiment appeared noisy, making it hard to justify any conclusions. Finally, the concentration dependency of the micelle kinetics was investigated. The two concentrations exhibited an equal growth and equilibrated at the same micelle size.

4.2 Future recommendations

The difficulties that accompany DLS shed light on the challenges of characterizing nanostructures. The small size scale makes it particularly hard to obtain information that is not distorted by either dust particles or aggregates.¹ For experiments that require DLS measurements over time it is advised to leave the sample sealed and to directly insert it in the instrument for the duration of the experiment. Pipetting and subsequent handling accumulates dust over time and leads to unreliable results. Even though DLS offers a fast and cheap way to detect trends, the high sensitivity of dynamic light scattering to the size of the particles further make it a contested choice for quantitative kinetic expressions.

More exact techniques such as small angle neutron scattering (SANS) could offer a fully picture of micelle growth but come at a high cost, especially considering the long relaxation time that is achieved with the rotator device. For future work using the rotator, increasing the interface turnover rate might both lead to more significant differences between samples and also decrease the characteristic relaxation times of

the micelles. Creating more interface per time per bulk volume can be achieved in different ways. First, different geometries can be used. Rectangular prisms can create large interfaces, even for vials that are barely filled. It is important to note that the difference between the 0° and 90° positions has to be maximized. An optimal situation would be with a long side parallel to and a small length perpendicular to the rotating axis. Whereas these geometries might not be readily available, cuvettes offer a good alternative. In conjunction with using cuvettes, a lower bulk volume can be used without sacrificing surface exposure. Furthermore, it is advised to keep bulk volumes as low as possible *i.e.*, vary samples filled from 10 to 30% instead of 25 to 75%. However, one has to be careful that the DLS laser is still able to travel through the bulk solution clear from any interference such as the meniscus. Combining these improvements, the ratio of interface turnover to bulk volume can be increased ~ 4-fold. Increasing the rpm is not encouraged as it might induce centrifugal forces.

Improvements can further be made to retrieve more reproducible results. The variance in micelle sizes obtained after cosolvent removal can be minimized by running the experiment for different batches. Additionally, if samples of different concentrations are required, it is advised to dilute from one mutual batch. Dialyzing the solutions also introduced some discrepancies between various mixtures. The swelling of the tubing and the subsequent dilution showed inconsistencies for different concentrations and were most likely artifacts from preparation. The determination of post-dialysis concentrations further introduced inaccuracies. In the future, the use of rigid tubing can prevent these drawbacks.

the rotator as a means to obtain an accurate quantification for surface turnover rates can be extended by further investigating the influence of temperature on micellar

systems. Temperature affects a wide range of system properties such as interfacial tension, viscosity, solvent quality, diffusivity etc. More specifically, it would be advantageous to alter the hydrophobic block to a more stable polymer. Polybutadiene is prone to degradation and cross-linking, especially upon heating. Other hydrophobic polymers such as poly(ethylene propylene) (PEP) offer a less susceptible alternative with a low glass transition temperature.^{2,3} Murphy and coworkers have previously examined the dependency of chain exchange on temperature using magnetic stirring.¹ It would be interesting to build forth on their hypothesis of slower exchange kinetics for increased temperatures as a result of an increased energetic barrier.¹ For this, using the rotator with the advised changes should provide sufficient surface turnover rates to obtain data on the relaxation behavior on a relatively short time scale (days). Additionally, using the PEP might help to prevent collapsing of the micelles at higher temperatures.

REFERENCES

1. Hiemenz, P. C.; Rajagopalan, R. Principles of colloid and surface chemistry, 3rd ed.; Eds.; CRC/Taylor & Francis: Boca Raton, FL, 1997
2. Murphy, R. P., Chain Exchange in Aqueous Solutions of Block Polymer Micelles. M.S. Thesis, University of Delaware, Newark, DE, 2014.
3. Won, Y.-Y.; Brannan, A. K.; Davis, H. T., Bates, F. S. Cryogenic transmission electron microscopy (cryo-TEM) of micelles and vesicles formed in water by poly(ethylene oxide)-based block copolymers. *Journal of Physical Chemistry B*, **2002**, 106, 3354-3364

Appendix

COPYRIGHT PERMISSION STATEMENT

Order Completed

Thank you for your order.

This Agreement between Laurens Heusele ("You") and The American Association for the Advancement of Science ("The American Association for the Advancement of Science") consists of your license details and the terms and conditions provided by The American Association for the Advancement of Science and Copyright Clearance Center.

Your confirmation email will contain your order number for future reference.

[Printable details.](#)

License Number	4101531494370
License date	May 03, 2017
Licensed Content Publisher	The American Association for the Advancement of Science
Licensed Content Publication	Science
Licensed Content Title	On the Origins of Morphological Complexity in Block Copolymer Surfactants
Licensed Content Author	Sumeet Jain, Frank S. Bates
Licensed Content Date	Apr 18, 2003
Licensed Content Volume	300
Licensed Content Issue	5618
Volume number	300
Issue number	5618
Type of Use	Thesis / Dissertation
Requestor type	Scientist/individual at a research institution
Format	Print and electronic
Portion	Figure
Number of figures/tables	1
Order reference number	
Title of your thesis / dissertation	Chain exchange kinetics of block copolymer micelles mediated by the air-water interface
Expected completion date	May 2017
Estimated size(pages)	65
Requestor Location	Laurens Heusele Hamlet Way NEWARK, DE 19711 United States Attn: Laurens Heusele
Billing Type	Invoice
Billing address	Laurens Heusele Hamlet Way NEWARK, DE 19711 United States Attn: Laurens Heusele
Total	0.00 EUR